BMC Plant Biology

RESEARCH

Open Access

Genome-wide identification, molecular docking and expression analysis of enzymes involved in the primary and secondary metabolic branching points of the selenium metabolic pathway in *Cardamine hupingshanensis*

Yue Xu[1,2†], Lilong Gao[1,2†], Jingyi Liu[2], Wenwu Guan[2], Jingyu Xie[1,3], Xixi Zeng[3], Yushan Chen[1,2], Yanke Lu[2], Zhi Hou[2], Zhixin Xiang[2], Yifeng Zhou[1,2*] and Qiaoyu Tang[1,3*]

Abstract

Background *Cardamine hupingshanensis* is a plant known for its unique selenium tolerance, making it a key model for selenium metabolism research. Adenosine phosphosulfate kinase (*APK*) and adenosine phosphosulfate reductase (APR) are widely distributed in plants and play a crucial role in selenium metabolism. While genome-wide analyses of the *APK* and *APR* families have been conducted across various plant species, a systematic identification and analysis of these gene families in *Cardamine hupingshanensis* is still lacking.

Results There are 7 *ChAPK* and 5 *ChAPR* genes identified from the genome of *C. hupingshanensis*, which can be classified into 4 subfamilies for *ChAPK* and 3 subfamilies for *ChAPR*, respectively. All these members share similar conserved motifs and gene structures. Phylogenetic and promoter analyses suggest they are involved in environmental responses, phytohormone regulation, and light signalling. Molecular docking analysis indicated that ChAPK enzymes have a higher affinity for adenosine phosphoselenate (APSe) compared to ChAPR. In 3D interaction force analysis, residues such as His^{80}, Asp^{134} and Arg^{137} were found to interact with the substrate APSe in ChAPK. For ChAPR, residues such as Gly^{226}, Arg^{313} and Leu^{150} were primarily involved in the catalytic site. Leaf cells of *C. hupingshanensis* exhibited a reduced state under 1 μg Se L^{-1} selenite concentration, but showed an oxidative state at 100 μg Se L^{-1}, as indicated by antioxidant enzyme activities and metabolite assays. The gene expression level of

†Yue Xu and Lilong Gao contributed equally to this work.

*Correspondence:
Yifeng Zhou
77416757@qq.com
Qiaoyu Tang
330375856@qq.com

Full list of author information is available at the end of the article

ChAPK2-1 and *ChAPR2* increased by 4.2- and 10.1-folds, respectively, in the reduced state of plant cells, with smaller increases in the oxidative state, *ChAPK2-1* increased by only 1.5-fold and *ChAPR2* by 5.2-fold.

Conclusions All members of ChAPK and ChAPR families have a strong affinity for APSe and are regulated by the redox state. However, only three members of *ChAPK* (*ChAPK1-1*, *ChAPK1-2*, and *ChAPK4-2*) are regulated by the redox state, and these are located in the chloroplast. Furthermore, low concentrations of selenium in the nutrient solution can promote antioxidant activity in the leaves of *C. hupingshanensis* seedlings, whereas high concentrations of selenium exhibit the opposite effect, as confirmed by the results of oxidative metabolite and antioxidant enzyme assays.

Keywords *Cardamine hupingshanensis*, Adenosine phosphosulfate kinase, Adenosine phosphosulfate reductase, Molecular docking, Gene expression

Introduction

Selenium is a vital trace element for both humans and animals, and it plays a multifaceted role in plant physiology, including stimulating growth and development, enhancing photosynthesis, and aiding in the detoxification of heavy metals, among other processes [1, 2]. Research has consistently demonstrated that selenium supplementation can significantly improve both the yield and quality of various crops. For instance, incorporating selenium into rice cultivation not only markedly increases yield but also enhances photosynthesis efficiency [3, 4]. Similarly, adding selenium to glutinous corn and soybeans improves their nutritional profile by enriching trace element content [5, 6]. Extensive studies on diverse plants such as *lettuce* [7], *celery* [8], and *Alhagi maurorum* Medik [9], have shown that optimal selenium supplementation can mitigate the concentration of harmful metal ions, increase the activity of key enzymes like superoxide dismutase (SOD) and peroxidase (POD), and boost the levels of non-enzymatic antioxidant compounds, thus effectively combating environmental stress. Moreover, selenium plays a pivotal role in alleviating various abiotic stresses, including those caused by salinity [10, 11], drought [12, 13], and extreme temperatures [14, 15]. Recent findings also suggest selenium's involvement in the regulation of crucial biological pathways, such as phospholipid biosynthesis, amino acid production, and starch and sucrose metabolism, underscoring its critical regulatory function in plant physiology [16]. Given its numerous benefits, selenium accumulation and tolerance in plants have become increasingly important areas of study. Research has focused on hyperaccumulators, which thrive in high selenium-rich environments without toxicity [17]. Among these, twenty-five species of hyperaccumulators have been identified within the *Astragalus* genus (milkvetch, Fabaceae) [18]. Other notable selenium hyperaccumulators are found in the genera *Stanleya* (Prince's plume, Brassicaceae), *Oonopsis* (goldenweed, Asteraceae), *Xylorhiza* (woody aster, Asteraceae), *Symphyotrichum* (white heath aster, Asteraceae), and *Cardamine* (Brassicaceae) [18, 19]. These plants are crucial for studying selenium accumulation and tolerance mechanisms, with some species capable of accumulating up to 15,000 mg/kg of selenium in their leaves [18]. Specifically, *C. hupingshanensis*, native to the Wuling Mountains in the Hunan and Hubei provinces of China, is a selenium hyperaccumulator of the Cruciferae family [20]. This plant can accumulate up to 1427 mg/kg of selenium in its leaves, making it an ideal model for researching selenium absorption, transport, and metabolism [20–23]. Seedlings were treated with selenite and a cDNA library was constructed for RNA sequencing, which yielded 48,989 unique genes, then differential expression analysis revealed that 25 genes had a significant response to selenium. Additionally, chromosomal-level genome assembly revealed that the plant has 16 chromosomes, laying the foundation for further research. Through integrated analysis of genome, transcriptome, and metabolome data, key biosynthetic pathways potentially associated with selenium tolerance were identified, including flavonoid compounds, glutathione, and lignin metabolism [24, 25]. Key enzymatic reactions in related metabolic pathways, such as adenosine triphosphate sulfurylase (ATPS) [26], selenomethionine cycle enzyme (SeMTC) [27], and selenocysteine synthase (SAT and OASTL) [28], have been studied, revealing their critical roles in selenium stress response and offering valuable insights into the selenium metabolic network in plants (Fig. 1).

Selenium is metabolized by plants through pathways primarily associated with sulfur (S) metabolism [2]. Selenium assimilation begins with the conversion of selenium by ATPS into APSe, which is subsequently phosphorylated by APK into 3'-phosphoadenosine-5'-phosphoselenate (PAPSe) [25]. This compound serves as a selenate donor for selenide synthesis in a secondary pathway. The reduction of APSe to selenite by APR marks a critical step, followed by a further reduction by sulfite reductase (SiR), leading to the formation of selenocysteine (SeCys) via O-acetyl serine (OAS) [29]. This initiates the primary pathway into the selenomethionine cycle, culminating in the synthesis of selenium-containing amino acids and peptides [25]. Thus, APSe is an important branch point

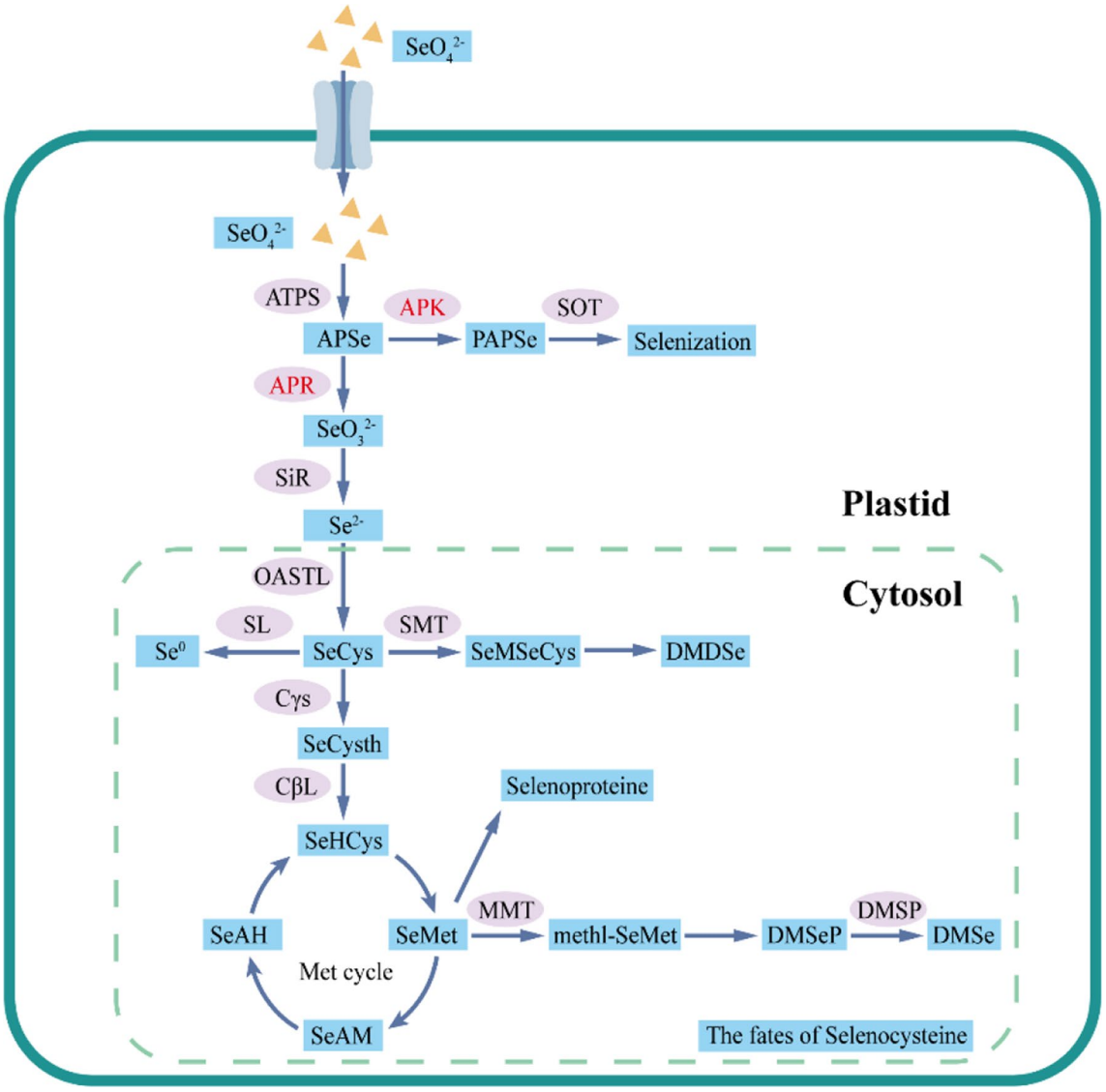

Fig. 1 Schematic diagram of selenium metabolism by Figdraw. ATPs: ATP sulfurylase; APSe: adenosine 5′-phosphoselenate; APK: adenosine 5′-phosphosulfate kinase; PAPSe: phospho adenosine phosphor-selenate; SOT: sulfotransferase; GLS: glucosinolates; Desulfo-GLS: desulfo-glucosinolates; PAP：adenosine 3'-phosphate-5'-phosphate; APR: adenosine 5′-phosphosulfate reductase; SiR: sulfite reductase; OAS: O-acetylserine; CS: Cysteine synthase; SeCys: selenocysteine; SeHCys: selenium homocysteine; SeMet: selenomethionine; SMT: selenocysteine methyltransferase; methl-SeMet: selenium methyl selenomethionine; SeMSeCys: selenomethylselenocysteine; DMDSe: dimethyl diselenide; SL: SeCyslyase; DMSe: dimethyl selenide

in plant selenium metabolism, with APK and APR utilizing APSe as a substrate and competing for its metabolism. Studies have shown that redox regulation of sulfur partitioning between these two branches is critical in the sulfur metabolic pathway, with sulfur partitioning in plants largely dependent on the activity of APK and APR. Their activities are regulated by the redox state to optimize catalytic efficiency in the reduced and oxidized forms, respectively [30, 31]. Given the chemical similarities between sulfur and selenium, analogous functions are likely to exist in the selenium metabolic pathway [25].

APK and APR are key enzymes at crucial branch points in plant selenium metabolism and are regulated by the redox environment. In a study of the onion (*Allium cepa L.*) *APK* sequence alignment, it was found that residues 1–63 form the P-loop domain, which is crucial for the binding of ATP and APS. Particularly, the residues R29, F37, and T38 directly participate in the binding of ATP and APS, providing a structural foundation for the functional study of APK [32]. In *A. thaliana*, the N-terminal region contains a redox-regulated switch, pivotal for their function, which involves an intermolecular disulfide bond between Cys86 of one monomer and Cys119 of another [30]. This bond is highly sensitive to redox changes; its reduction not only enhances the catalytic efficiency (kcat/Km) by 17-fold but also reduces substrate

inhibition by 15-fold, thus optimizing the enzyme activity in response to cellular redox states [30]. Further studies show that *APK* in *A. thaliana* exists in both reduced and oxidized forms, reflecting its functional adaptability to the intracellular redox environment. Titration methods have determined the midpoint redox potential of the disulfide in AtAPK to range between – 295 mV and – 286 mV at pH 7.5 and between – 260 mV and – 249 mV at pH 7, indicating its functional adaptability to the intracellular redox environment [29, 33]. Additionally, a similar redox regulatory mechanism to that *APK* in *A. thaliana* was also found in rice (*OsAPK1*), which similar disulfide bond conserved sites (C36 and C69) were also found [34]. Site-directed mutagenesis and in vitro enzyme activity assays revealed that the enzyme activity of OsAPK1 is influenced by the oxidative environment, and the mutant exhibited different activity changes compared to the wild-type [34]. This further indicates the importance of disulfide bonds in the redox regulation mechanism of *APK*, and suggests that this regulatory mechanism is conserved across different plant species. Studies have shown that the activity of APR in *A. thaliana* is regulated by redox conditions. As an important antioxidant, reduced glutathione (GSH) maintains the reduced cellular environment at high concentrations, during which APR activity is low; in an oxidative environment, GSH is oxidized glutathione (GSSG), leading to a decrease in the GSH/GSSG ratio, which subsequently enhances APR activity. Therefore, it has been confirmed that APR activity is closely related to the oxidation state of the GSH pool [35–37]. The redox potential of AtAPR is approximately – 330 mV at pH 8.5 [35, 38]. Additionally, structural analysis of AtAPR indicates that each monomer contains an N-terminal [4Fe-4S] cluster domain and a C-terminal GRX-related domain [31, 39, 40]. This structural feature has also been verified in the crystal structure of *Mycobacterium tuberculosis* (*MtbAPR*) [41].

Although research on *APK* and *APR* has made significant progress in various plants, no related studies have been conducted in *C. hupingshanensis*. To fill this gap, this study employs bioinformatics methods to first identify the *APK* and *APR* genes from the genome of this plant, and conduct a systematic analysis of their physicochemical properties, basic functions, and substrate docking simulations. Genes associated with selenite-induced oxidative stress responses were also screened. It is hypothesized that similar redox regulation might exist between two branches of selenium metabolism, providing new perspectives for understanding the selenium metabolic network in plants.

Materials and methods

Genome-wide identification of *APK* and *APR* genes

The genome data of *A. thaliana* and *C. hupingshanensis* were obtained from the *Arabidopsis* Information Resource (TAIR, https://www.arabidopsis.org/) and the *C. hupingshanensis* Genome Database (accession number PRJCA005533), respectively. Homologous protein sequences of *C. hupingshanensis* were extracted using the Blast Zone function of TBtools software (BlastType: blast, Outfmt: Table) [42], with AtAPK and AtAPR protein sequences from *A. thalianan* as templates. Candidate genes were then screened and validated using NCBI BLAST (https://blast.ncbi.nlm.nih.gov/blast/Blast.cgi) [74] and Conserved Domain Search (https://www.ncbi.nlm.nih.gov/Structure/cdd/wrpsb.cgi) [75]. The physicochemical properties and subcellular localization of *ChAPK* and *ChAPR* gene family members were analyzed using the online tools ExPASy (https://web.expasy.org/protparam/) and WoLF PSORT (https://www.genscript.com/wolf-psort.html) [43, 76], respectively.

Chromosomal distribution and domain analysis of *APK* and *APR* genes

Chromosomal localization information for *APK* and *APR* gene family members in *C. hupingshanensis* was extracted and visualized using the TBtools software [42]. Conserved motifs, gene structures, and conserved domains of *ChAPK* and *ChAPR* were analyzed using MEME [77], GFF annotation files, and the Pfam database [78]. The results were visualized using "Gene Structure View (advanced)" in TBtools. Multiple sequence alignments were performed using ClustalW [79], and the results were visualized and refined using ESPript 3.0 (https://espript.ibcp.fr/ESPript/cgi-bin/ESPript.cgi) and Adobe Illustrator [44].

Phylogenetic analysis of *APK* and *APR* genes

To reveal their relationship between the *ChAPK* and *ChAPR* gene families and those in other species, the protein sequences of APK and APR from *A. thaliana*, *Brassica oleracea*, *Brassica napus*, *Capsella rubella*, *Linum usitatissimum*, *Thellungiella halophila*, *Secale cereale*, *Oryza sativa*, *Zea mays*, *Glycine max*, *Arachis hypogaea*, *Populus trichocarpa*, *Vitis vinifera*, and *Prunus mume*, downloaded from NCBI, were aligned with those from *C. hupingshanensis*. The amino acid sequences were aligned using Clustal W, and the maximum likelihood (ML) method was used to construct a phylogenetic tree using MEGA 11.0 software [45]. The phylogenetic tree was refined and visually enhanced using the Evolview online tool (https://www.evolgenius.info/evolview-v2) [80], and gene names were assigned based on their evolutionary relationships with *A. thaliana*.

Homology modeling and ligand preparation

The secondary structures of APK and APR proteins in *C. hupingshanensis* were predicted using the SOPMA online tool [46]. The most suitable crystal structure templates were identified and selected from the SWISS-MODEL template database (https://swissmodel.expasy.org/). The structural formulas of adenosine triphosphate and 5'-O-[(Selenonooxy) phosphinato] adenosine were retrieved from the ChemSpider database and redrawn using Kingdraw. Protein active sites of APK and APR in *C. hupingshanensis* were predicted using the PrankWeb tool [47].

Molecular docking

Molecular docking simulations for APK and APR proteins of *C. hupingshanensis* were performed using AutoDock v4.2 [48]. Proteins and ligands were preprocessed, and docking exhaustiveness was set to 10. The best ligand conformations were selected based on the lowest binding energy. Hydrogen bonds and hydrophobic interactions were analyzed and visualized using PLIP and PyMol [49–51], while binding energy data were graphically represented using GraphPad Prism 10.1.2 [52].

Plant cultivation and sample preparation

Seeds of *C. hupingshanensis* used in this study were collected from the Yutangba Color Mine in Enshi, Hubei Province, China (latitude: 30.3860918, longitude: 109.2890204), and subsequently cultivated under laboratory conditions. These plants are wild-type and non-endangered species, in compliance with the IUCN Policy Statement on Research Involving Endangered Species and the Convention on International Trade in Endangered Species of Wild Fauna and Flora (CITES), as well as relevant laws and regulations. The plant materials were identified by Professor Yongmei Yi, and voucher specimens were deposited in the National Plant Specimen Resource Center at the College of Life Sciences, Hunan Normal University, under the accession number HNNU00063178. Seedlings were grown in a plant growth chamber under controlled conditions at 22 ± 1°C with a 16-hour photoperiod and a light intensity of 1500 μmol m^{-2} s^{-1}. Ninety-six seedlings, approximately 10 cm in height after four months of cultivation, were selected as experimental samples. Roots were rinsed with running water and equilibrated in Hoagland nutrient solution for 2 days before treatment with varying selenium concentrations (1 μg Se L^{-1}, 10 μg Se L^{-1}, and 100 μg Se L^{-1}), with 0 μg Se L^{-1} serving as the control. Sodium selenite (Na_2SeO_3) was used as the selenium source. Leaf samples were collected from three seedlings at various time points (1, 3, and 5 d) and hourly intervals (3, 6, 12, and 24 h), rapidly frozen in liquid nitrogen, and stored at -80 °C for redox index measurement and RNA extraction. Three biological replicates were set up for each sample.

Extraction and quantification of antioxidant enzyme activity

A 0.1 g fresh plant sample was homogenized with 1 mL of extraction buffer containing 25 mmol L^{-1} phosphate buffer (pH 7.8), 0.2 mmol L^{-1} EDTA, and 2% (w/v) PVPP. The homogenate was centrifuged at 12,000 rpm for 20 min at 4 ℃. The supernatant was collected for enzyme activity assays. Activities of three enzymes, catalase (CAT) [53], POD [54], and SOD [55], were measured for each sample, and results normalized based on fresh weight and reaction time.

Determination of oxidized metabolites

Fresh leaf tissues were homogenized in 1% (w/v) trichloroacetic acid (TCA) and centrifuged at 10,000×g for 10 min at 4 °C. The supernatant was mixed with 10 mM potassium phosphate buffer (pH 7.0) and 1 M potassium iodide (KI). Hydrogen peroxide (H_2O_2) concentration in the supernatant was measured at 390 nm, and the results were expressed as μmol/g fresh weight [56, 57].

A 0.15 g fresh leaf tissue sample was homogenized in 1.5 mL of a mixture containing 20% thiobarbituric acid (TBA) and 0.5% TCA and incubated at 95 °C for 45 min. After cooling, the sample was centrifuged at 4,000×g for 35 min at 4 °C. The supernatant was collected, and the absorbance was measured at 532 nm and 600 nm. The absorbance at 600 nm was subtracted from that at 532 nm to account for background interference, and the malondialdehyde (MDA) concentration was calculated using the molar extinction coefficient of 155 mM^{-1} cm^{-1} at 532 nm [58].

GSH and GSSG levels were measured using assay kits provided by Shanghai Sangon Biotechnology Co., Ltd.

Gene expression analysis

Total RNA was extracted from leaves using the *TransZol*™ Up Plus RNA Kit (TransGen Biotech, China). RNA concentration and quality were assessed using a NanoDrop 2000 (Thermo Fisher Scientific, USA), and its integrity and potential gDNA contamination were verified by 1.0% agarose gel electrophoresis. cDNA synthesis was performed using the HiScript III RT SuperMix for qPCR kit (Vazyme, China). Real-time quantitative PCR (qRT-PCR) was conducted on an ABI StepOne Plus system (Thermo Fisher Scientific, USA), using the Hieff qPCR SYBR Green Master Mix (Yeasen Biotechnology (Shanghai) Co., Ltd.) to measure target gene expression levels. Relative expression was calculated using the $2^{\wedge-\Delta\Delta CT}$ method [59] Results were analyzed and visualized using GraphPad Prism 10.1.2 [52]. All experiments were repeated three times, and statistical significance was evaluated

using one-way ANOVA followed by LSD tests ($p < 0.05$) [52]. All analyses were performed in triplicate. For qRT-PCR analysis, *ChActin* was used as the reference gene. The primers for Actin were as follows: Forward: 5'-GGTACTGAGGGAAGCCAAGA-3', Reverse: 5'-GGAATCGCCGACAGAATG-3'. The primers for other genes are listed in Supplementary Table S2.

Results

Identification and analysis of *APK* and *APR* genes in *C. hupingshanensis*

A total of 7 *ChAPK* genes and 5 *ChAPR* genes within the *C. hupingshanensis* genome were identified using the *A. thaliana* genome sequence as a reference. To systematically analyze the physicochemical properties of the encoded proteins, we evaluated the *ChAPK* and *ChAPR* gene family sequences in terms of amino acid count, molecular weight, isoelectric point, average hydrophilicity, instability coefficient, lipid affinity, and subcellular localization in Table 1. The coding sequences and protein sequences of ChAPK and ChAPR genes are shown in Table S1. The ChAPK protein sequences display significant length variation, ranging from 248 to 291 amino acids, with ChAPK2-1 and ChAPK2-2 being the longest and ChAPK3 the shortest. In contrast, the lengths of the ChAPR protein are relatively consistent. The average molecular weights of the ChAPK and ChAPR proteins are 43.79 kDa and 30.73 kDa, respectively. The isoelectric points (pI) of the ChAPK proteins vary from 7.52 to 9.17, classifying them as alkaline. In comparison, the pI of ChAPR proteins range from 6.02 to 7.05, with only ChAPR1-2 and ChAPR2 exhibiting a pI values above 7, suggesting a minority of them behave alkalinely. The lipid affinity indices for ChAPK and ChAPR proteins range from 81.41 to 87.92 and 84.13 to 88.52, respectively. The average hydrophilicity (GRAVY) for ChAPK proteins ranges from −0.481 to -0.226, while ChAPR proteins show values between −0.328 and −0.271, indicating that both gene families produce hydrophilic proteins, as all values are negative. Both families also exhibit lipid affinity indices below 100, further suggesting a hydrophilic nature. Stability analysis reveals that three ChAPK proteins have instability coefficients below 40, indicating they are relatively stable, while all ChAPR proteins are deemed unstable. Subcellular localization predictions, based on UniProt, reveal that, except for ChAPK3 (which is cytoplasmic), most ChAPK proteins are localize to chloroplasts—a feature shared by all ChAPR proteins.

Chromosomal distribution and domain analysis *APK* and *APR* genes in *C.hupingshanensis*

The *ChAPK* and *ChAPR* genes are unevenly distributed across the seven chromosomes of *C.hupingshanensis*, primarily located on chromosomes 2, 4, 5, 6, 7, 15, and 16 (Fig. 2). Notably, chromosome 5 harbors two *APK* genes, namely *ChAPK1-2* and *ChAPK3*, while chromosome 2 contains a single *APK* gene, *ChAPK1-1*. Additionally, chromosome 7 has *ChAPR2* and the remaining chromosomes feature one *APK* gene and one *APR* gene each.

To further study the diversity of changes in the *ChAPK* and *ChAPR* gene families during evolution, the conserved sequences of the seven ChAPK and five ChAPR proteins were analyzed using MEME online software (Fig. 3). Twelve conserved motifs (named motifs 1–12) were identified in the ChAPK protein family, while the ChAPR protein family exhibited 11 different conserved motifs (named motifs 1–11). All ChAPK protein proteins shared seven common motifs (motifs 3, 9, 1, 8, 2, 4, and 5) in the same order, although some motifs were unique to specific subgroups. For example, motif 6 was predominantly found in ChAPK subgroup I, motif 12 was exclusive to subgroup IV, and subgroups III contained motifs 7 and 11. This motif distribution suggests that genes with similar motif structures are clustered in the same branch

Table 1 The physicochemical properties of APK and APR proteins in *C. hupingshanensis*

	Gene ID	Gene name	Length (aa)	Molecular weight (kD)	pI	GRAVY	Instability index	Aliphatic index	Subcellular localization
APK	Chu050222	ChAPK1-1	273	51.81105	8.52	-0.245	23.42	84.65	chloroplast
	Chu021196	ChAPK1-2	273	52.05044	8.03	-0.244	24.92	84.29	chloroplast
	Chu026696	ChAPK2-1	291	50.65118	7.52	-0.299	47.14	84.47	chloroplast
	Chu017254	ChAPK2-2	291	50.77084	7.52	-0.273	43.61	87.15	chloroplast
	Chu023700	ChAPK3	248	50.75974	8.59	-0.481	50.94	81.41	cytoplasm
	Chu041556	ChAPK4-1	289	29.57292	9.17	-0.264	41.39	86.06	chloroplast
	Chu012712	ChAPK4-2	284	29.52582	8.64	-0.226	33.9	87.92	chloroplast
APR	Chu039343	ChAPR1-1	467	32.03246	6.02	-0.303	47.96	84.13	chloroplast
	Chu010439	ChAPR1-2	467	32.03047	7.02	-0.328	44.77	85.35	chloroplast
	Chu006667	ChAPR2	451	27.821	7.05	-0.303	47.46	84.75	chloroplast
	Chu028270	ChAPR3-1	458	31.79138	6.65	-0.271	43.18	88.52	chloroplast
	Chu018765	ChAPR3-2	458	30.99134	6.18	-0.28	43.75	87.66	chloroplast

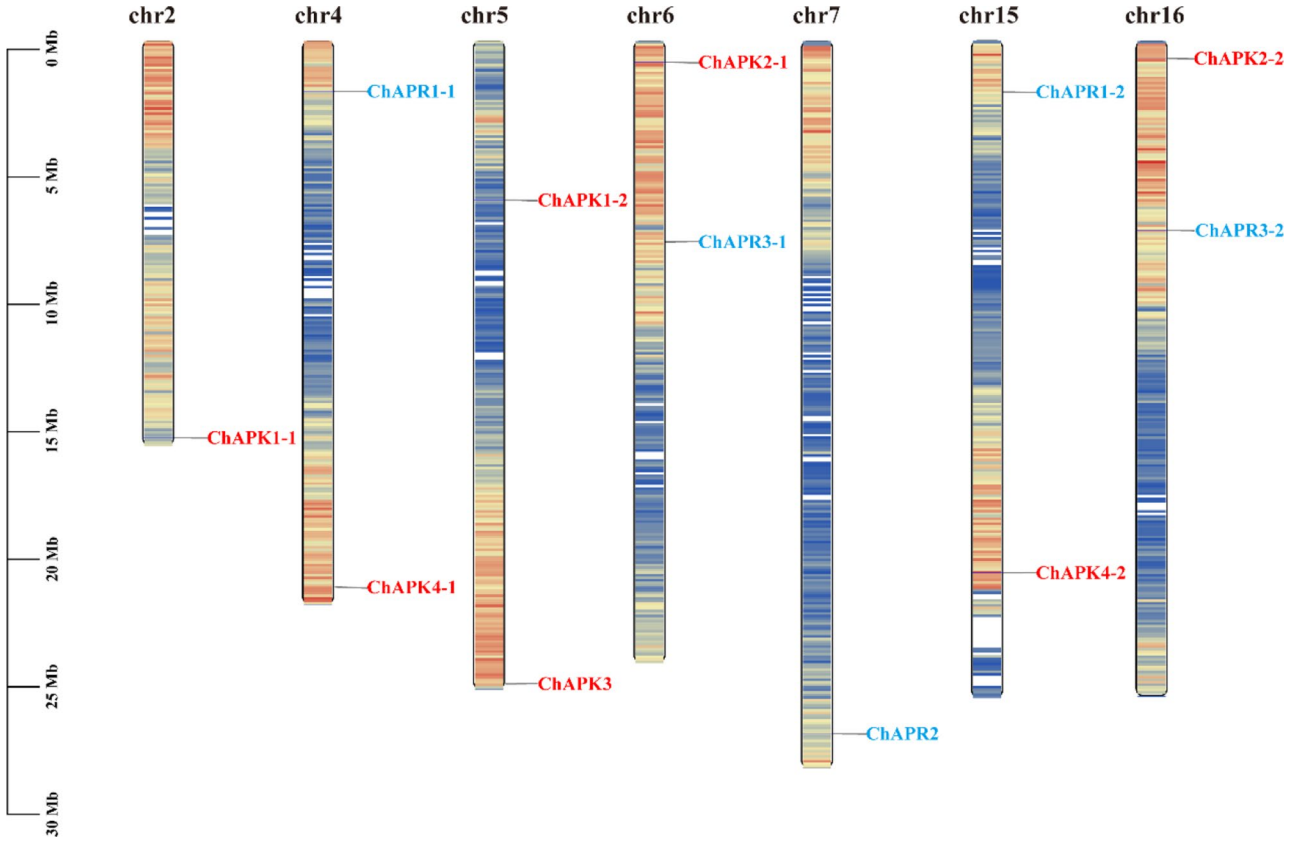

Fig. 2 Chromosomal distribution of *APK* and *APR* genes in *C. hupingshanensis*. The chromosome numbers are shown on the left side of each strip

of the APK family phylogenetic tree. The ChAPR protein family exhibited high conservation, with all members displaying the same 10 motifs (motifs 8, 11, 9, 5, 2, 10, 3, 1, 7, 4, and 6) in a consistent order.

To further examine the structural similarities and differences between *ChAPK* and *ChAPR* genes, a structural diagram was constructed based on the genome sequence of *C. hupingshanensis*, which included both untranslated regions (UTRs) and coding regions (CDS), in conjunction with the phylogenetic tree (Fig. 3). A comparison of exons and introns revealed that the *ChAPK* gene family contains more exons and introns than the *ChAPR* gene family (Fig. 3). Specifically, the seven *ChAPK* genes each contain six introns and seven exons, with the exceptions of *ChAPK4-1* and *ChAPK4-2*. In contrast, the five *ChAPR* genes generally include untranslated regions (UTRs), except for *ChAPR1-1* and *ChAPR3-2*, which have fewer introns and exons than other family members. Conserved structure analysis using the NCBI Pfam database showed that the *ChAPK* gene family contains an adenylylsulfate kinase domain (APS_kinase, PF01583), which may be related to motifs 1, 2, 3, 4, 8, and 9. The *ChAPR* gene family contains two domains: the phosphoadenosine phosphosulfate reductase family (PAPS_reduc, PF01507) and the thioredoxin-like superfamily (Thioredoxin_like superfamily).

Sequence alignment of the ChAPK protein revealed five highly conserved amino acid motifs. The first region is the N-terminal structure (^{80}NIKWHECSVEKV-DRQRLLD^{98}) (Fig. S1), which is an unstructured loop containing an α-helix of approximately seven amino acids [30]. This region plays a redox regulation through the formation of an intermolecular disulfide bond between one monomer and the N-terminal region of another monomer, specifically between Cys86 and Cys119 [60]. The P-loop (^{108}GLSGSGKST^{116}) and the DxxG domain (^{216}DPKG^{220}) are also conserved, with the P-loop located near the N-terminal, between the β-sheet and α-helix, and the DxxG domain near the C-terminus. Together, these motifs form a nucleotide-binding domain that corresponds to the GxxxxGK—DxxG signature of GTP/ATP binding domain [61, 62]. Another important conserved motif is the DGDN-loop (^{136}DGDN^{139}), where Asp136 and Asp138 are involved in binding APS and ATP·Mg^{2+}, which is crucial for the catalytic activity of *AtAPK*. Therefore, it can be speculated that this motif may also play an important role in the catalytic activity of *APK* genes in *C.hupingshanensis* [30]. Finally, the ENIRRVGEVA structural region is relatively conserved, except for mutations

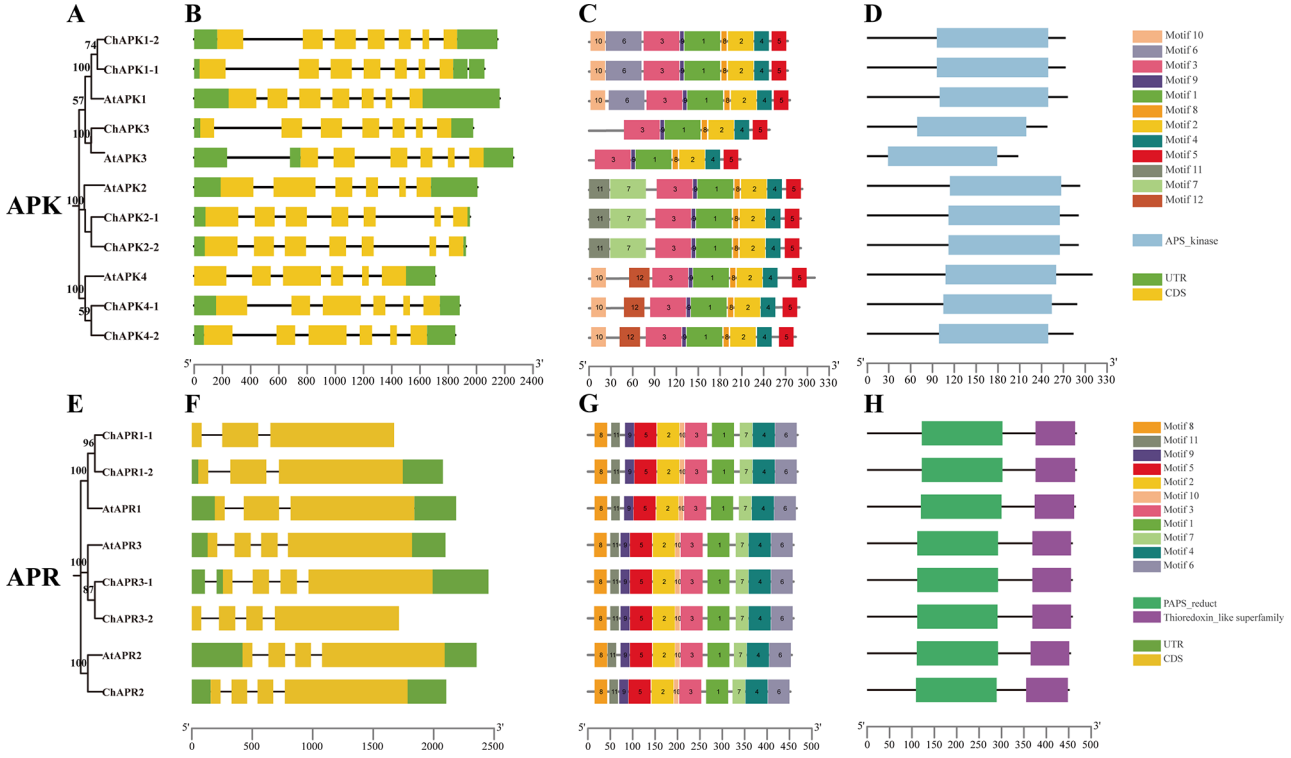

Fig. 3 Phylogenetic trees, motif, domain, and gene structure of the *APK* and *APR* genes. (**A, E**) The phylogenetic tree; (**C, G**) Conserved motifs of the proteins, motifs and the numbers inside the rectangles correspond to specific motifs, for example, Motif 1 is represented by "1"; (**D, H**) domains of the proteins, different colors represent different domains. (**B, F**) Exon-intron structures; exons are indicated by yellow boxes, and introns are indicated by lines.

at amino acid position 162 in *AtAPK2*, *ChAPK2-1*, and *ChAPK2-2*, although the function of this region remains undetermined.

Sequence comparison of ChAPR proteins revealed a binding [4Fe-4S] cluster in the N-terminal structural domains (amino acids 73–327) with APR activity, as well as a redox-active CXXC motif (^{385}CPFC^{388}) in the C-terminal structural domains (amino acids 328–465) [31, 40, 63]. The entire protein sequence contains seven conserved cysteine residues, five of which are located in the N-terminal structural region, including the four residues constituting the [4Fe-4S] cluster and the catalytic residue in a relatively conserved motif (^{321}XGGLH^{325}). The remaining two cysteine residues are located in the C-terminal structural region.

Phylogenetic analysis of *APK* and *APR* genes in *C. hupingshanensis*

The phylogenetic tree of *APK* and *APR* gene families in *C. hupingshanensis* (*ChAPK/ChAPR*), *A. thaliana* (*AtAPK/AtAPR*), *B. oleracea* (*BoAPK/BoAPR*), *B. rapa* (*BrAPK/BrAPR*), *C. rubella* (*CrAPK/CrAPR*), *C. sativa* (*CsAPK/CsAPR*), *E. salsugineum* (*EsAPK/EsAPR*), *L. rigidum* (*LrAPK/LrAPR*), *O. sativa* (*OsAPK/OsAPR*), *Z. mays* (*ZmAPK/ZmAPR*), and *G. max* (*GmAPK/GmAPR*) *P. trichocarpa* (*PtAPK/PtAPR*), *V. vinifera* (*VvAPK/VvAPR*), *P. mume* (*PmAPK/PmAPR*) and *Arachis hypogaea* (*AhAPK/AhAPR*) revealed that *APKs* clustered into four main groups, while *APRs* were categorized into three major groups (Fig. 4). Notably, *ChAPK* and *ChAPR* genes were more closely related to their orthologs in *A. thaliana*, *C. rubella* and *C. sativa*, suggesting that these gene families may have undergone a similar evolutionary process in these species. Additionally, the phylogenetic distribution suggests that the diversification of the *APK* and *APR* families likely occurred after the divergence of monocots and dicots. Furthermore, the fact that *C. hupingshanensis* and *A. thaliana* clustered in the same branch supports the idea that these species share a close evolutionary relationship and have undergone similar evolutionary trajectories.

Collinearity and evolution analysis of *ChAPK* and *ChAPR*

To elucidate the evolutionary relationships of the *APK* and *APR* genes in *C. hupingshanensis*, we performed collinearity analyses both within its genome and between its genome and that of *A. thaliana*. Intra-genomic collinearity analysis of *C. hupingshanensis* revealed that three pairs of *ChAPK* genes, indicated by red lines, exhibited segmental duplication (Fig. 5A). Additionally, collinearity analysis of the *ChAPR* gene family identified 10 segmental duplication events (Fig. 5C). Inter-species collinearity

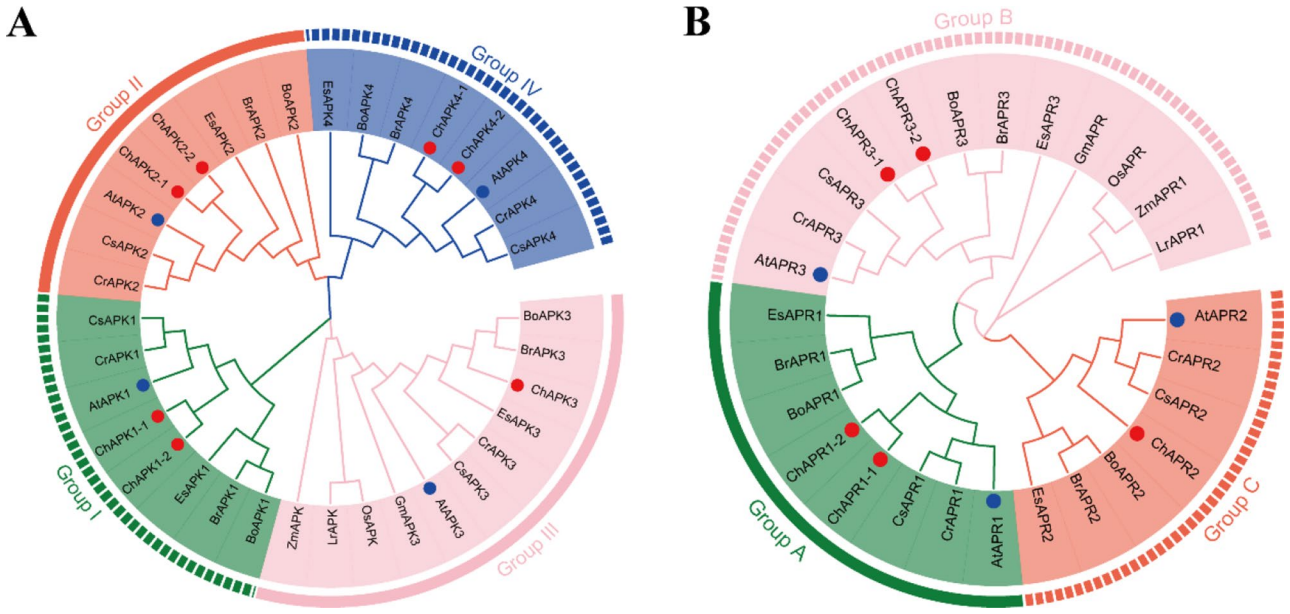

Fig. 4 Phylogenetic tree of APK and APR genes. The phylogenetic tree from *Arabidopsis thaliana* (At), *Brassica oleracea* (Bo), *Brassica rapa* (Br), *Capsella rubella* (Cr), *Camelina sativa* (Ca), *Eutrema salsugineum* (Es), *Lolium rigidum* (Lr), *Oryza sativa* (Os), and *Zea mays* (Zm) *Populus trichocarpa* (Pt), *Vitis vinifera* (Vv), *Prunus mume* (Pm), *Arachis hypogaeaand* (Ah) and *C. hupingshanensis* (Ch). (**A**) The phylogenetic tree of *APK*. (**B**) The phylogenetic tree of *APR*.

analysis indicated that the *ChAPK* gene family has one homologous gene in *A. thaliana*, while the *ChAPR* has three homologous genes (Fig. 5B and D). These results suggest that, during long-term evolution, several genes may have undergone sequence mutations, recombination, loss, or functional changes, resulting in only a few homologous genes between the two species.

Prediction of Cis-acting elements in the *ChAPK* and *ChAPR* families

Cis-acting elements were predicted in the 2000 bp upstream promoter regions of the *ChAPK* and *ChAPR* genes. A total of 159 cis-acting elements were identified in the *ChAPK* genes, while 106 were identified in the *ChAPR* genes, and these elements were classified into four major types (Fig. 6A,B). Among these, light-responsive elements, plant hormone regulatory elements, and abiotic stress-responsive elements were predominant (Fig. 6C,D). Notably, anaerobic induction elements (ARE) were widely distributed across both gene families. The promoter regions of light-responsive genes were mainly enriched with key elements such as G-box and Box4 motifs. As a core element in the ABA signaling pathway, ABRE was commonly found in *ChAPK* genes, suggesting its role in regulating genes involved in drought and high salinity stress. Additionally, *ChAPRs* contained typical MeJA-responsive elements, including the TGACG-motif and CGTCA-motif. These elements are associated with the jasmonic acid signaling pathway and are likely involved in regulating the expression of defense-related genes under both biotic and abiotic stress conditions. In summary, the identified cis-acting elements synergistically regulates gene expression, in response to various stress conditions, thereby enhancing plant survival and adaptability (Fig. 6).

Secondary and tertiary structures prediction of APK and APR enzymes

The secondary structures of ChAPK and ChAPR proteins were predicted using the SOPMA online tool. The analysis revealed that the protein sequences of both gene families are mainly composed of α-helices, β-sheets, extended links, and random coils. Among these, α-helices and random coils are more prevalent, while β-sheets are less common, indicating certain structural differences within the ChAPK family and some variations in the ChAPR protein, as shown in Table 2. To visualize the three-dimensional (3D) structures of ChAPK and ChAPR proteins, we used SWISS-MODEL online software for homology modeling. The crystal structures of *A. thaliana* adenosine phosphate sulfate kinase (APK ID: 4fxp.2.A) and adenosine phosphate sulfate reductase (APR ID: 2goy.1.A) were used as templates. The quality of the structural models was assesseding by comparing them to these reference templates. The sequence homology of the ChAPR proteins exceeds 72.87% with a coverage rate of over 0.62. Additionally, the GMQE and QMEAN scores are close to 1, indicating high overall model quality. However, the sequence homology, coverage, and GMQE of the five ChAPR protein models are relatively lower. Despite, the ERRAT scores for all the seven ChAPK and ChAPR protein models exceed 90, the VERIFY3D scores are

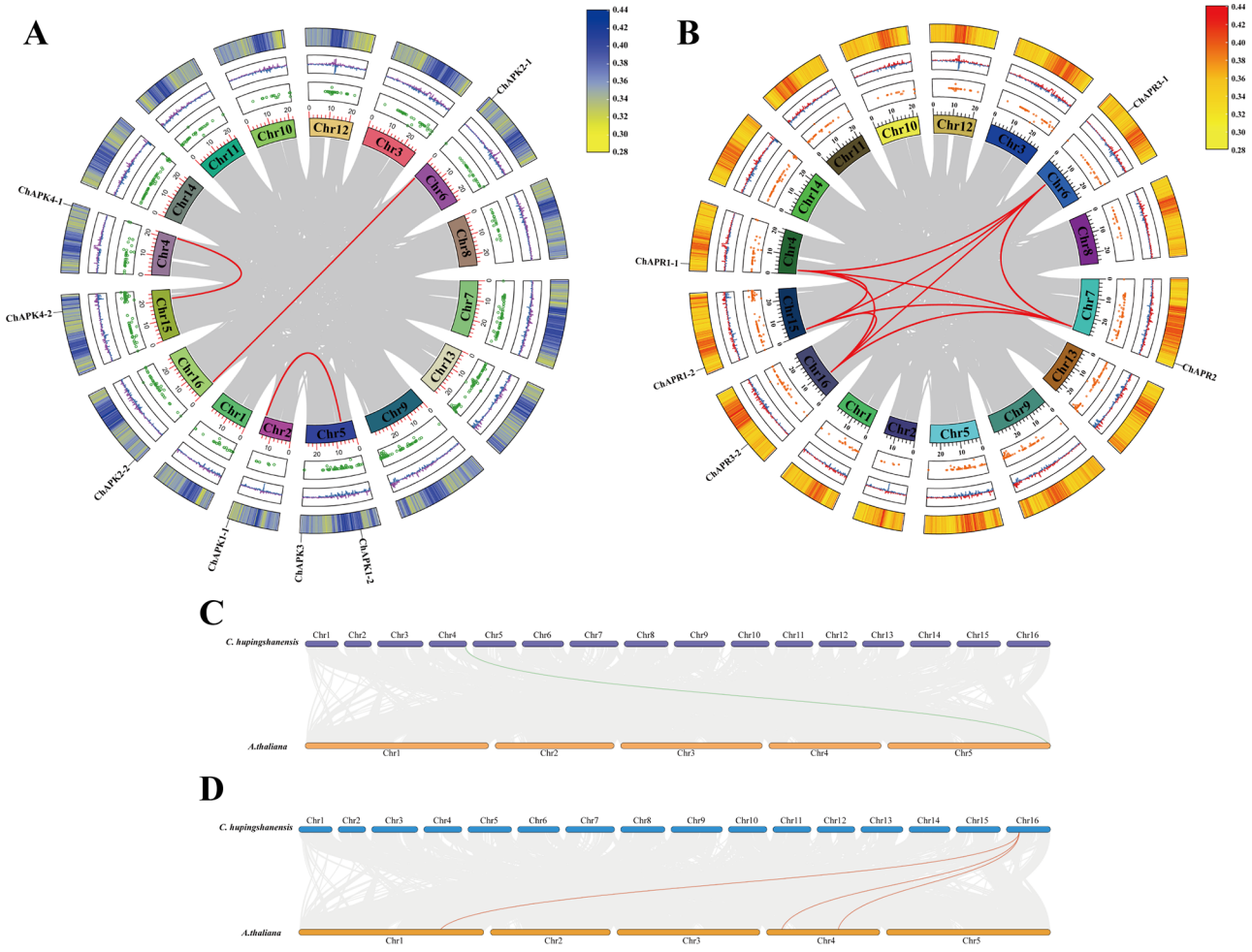

Fig. 5 Intragenomic collinearity map of *ChAPK* and *ChAPR*. (**A, B**) Intragenomic collinearity map of *ChAPK* and *ChAPR*. From the inner to outer of the Circos plot, gray lines in the background represent collinear blocks of *C. hupingshanensis* and *A. thaliana* genomes, while red lines emphasize collinear gene pairs within the *ChAPKs* and *ChAPRs*; the plot also includes a point plot for N-ratio distribution; a line plot for GCskew; a heatmap for gene density profile, and a line plot for GC ratio variation; labeled tags for a gene family. (**C, D**) Synteny analysis of *APK* and *APR* genes between *C. hupingshanensis* and *A. thaliana*. Green and red lines represent collinear pairs of *APK* and *APR* genes, respectively. Gray lines indicate all synteny blocks in the genome.

around 70%, and the G-factors are all greater than – 0.5. These metrics suggest that the homology models are of high accuracy and reliability. Therefore, the predicted structures can be used for further studies.

Molecular docking

The Prankweb online server was used to predict the ligand binding sites of ChAPK and ChAPR proteins. For the ChAPK protein family, nine potential binding pockets were predicted, while the number of binding sites for members of the ChAPR protein family ranged from 1 to 35 (Figs. 7 and 8). The top nine binding sites, based on their scores, were selected for further analysis. AutoDock Vina software was then used to simulate protein-ligand interactions and record the molecular docking binding energy. The results showed that the binding energy of ChAPK to APSe ranged from – 3.9 to -8.9 kcal·mol^{-1}, with the highest binding energies observed at site 1 and site 2. Among these, ChAPK3 exhibited the strongest binding energy with APSe (-8.9 kcal·mol^{-1}), outperforming other ChAPK members. In contrast, the highest binding energies of ChAPR to APSe varied more widely, ranging from 26.7 to -8.3 kcal·mol^{-1}, with the sites with highest binding energies being more dispersed across different binding sites.

To further study protein-ligand interactions, molecular docking technology was used to predict the binding affinity and binding mode between the protein and ligand. The 3D interaction display of the docked complex revealed multiple key interactions between the proteins and APSe, including hydrogen bonds, π bonds, and salt bridges. The overall structure of ChAPK and ChAPR is shown in Fig. 8. For example, in *ChAPK1-1*, the catalytic site (CS) coincides with the maximum affinity binding site (MBS), the amino acid residues within the P-loop (Gly^{107}-Thr^{112}) form a robust hydrogen bond network with the selenate

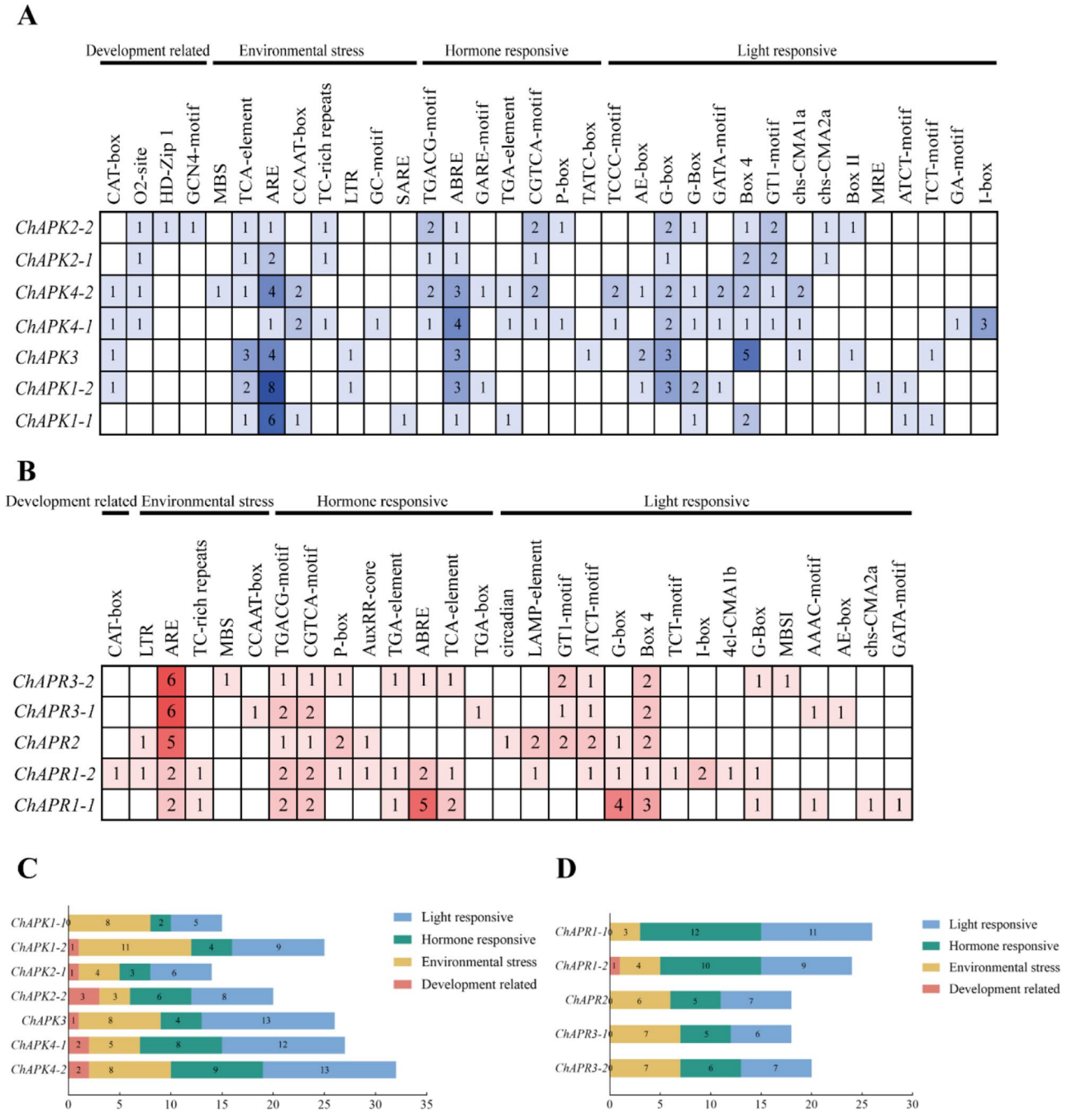

Fig. 6 Prediction of cis-acting elements in the promoter region in *ChAPKs* and *ChAPRs*. (**A, B**) represent the number and type of cis-regulatory element in *ChAPK* and *ChAPR*, respectively. (**C, D**) Quantitative statistics of major cis-acting elements in genes. (ARE: cis-acting regulatory element essential for the anaerobic induction; G-box: cis-acting regulatory element involved in light responsiveness; Box4: part of a conserved DNA module involved in light responsiveness; motifs. ABRE: cis-acting element involved in the abscisic acid responsiveness; TGACG-motif: cis-acting regulatory element involved in the MeJA-responsiveness; CGTCA-motif: cis-acting regulatory element involved in the MeJA-responsiveness).

group, strengthening the interaction between the selenate group and the enzyme. His^{80} and Lys$^{110/214}$ form stable salt bridges with the α-phosphate group, facilitating the precise positioning between the substrate and the enzyme. The carboxyl oxygen of Asp^{134} and Asn^{76} in the DGDN-loop form hydrogen bond interactions with the 2'-OH and 3'-OH groups of the APSe ribose, respectively. The adenine ring strengthens binding stability by hydrogen bonding with Asn^{154}, Ser^{178}, and Ile^{177}, while Arg^{151} forms additional stabilizing interactions with the NH_2 group of the adenine ring. Additionally, the guanidino nitrogen atom of Arg^{137} forms a π-π interaction with the

Table 2 Validation of the modelled structures of ChAPK and ChAPR

Gene	Template	Sequence identity	Coverage	GMQE	QMEAN	Alpha helix	Beta turn	Extended strand	Random coli
ChAPK1-1	4fxp.2.A	92.50%	0.73	0.7	0.91	34.07%	5.86%	19.78%	40.29%
ChAPK1-2	4fxp.2.A	93.00%	0.73	0.7	0.9	30.77%	6.23%	20.15%	42.86%
ChAPK2-1	4fxp.2.A	77.16%	0.68	0.62	0.87	29.21%	7.56%	17.87%	45.36%
ChAPK2-2	4fxp.2.A	77.16%	0.68	0.62	0.86	34.36%	6.87%	18.90%	39.86%
ChAPK3	4fxp.2.A	72.87%	0.8	0.74	0.86	35.89%	5.65%	17.34%	41.13%
ChAPK4-1	4fxp.2.A	74.87%	0.69	0.62	0.85	31.83%	5.88%	16.61%	45.67%
ChAPK4-2	4fxp.2.A	77.16%	0.69	0.63	0.86	30.99%	5.28%	14.79%	48.94%
ChAPR1-1	2goy.1.A	54.17%	0.51	0.4	0.76	40.90%	6.85%	13.28%	38.97%
ChAPR1-2	2goy.1.A	52.26%	0.52	0.4	0.75	39.40%	6.00%	14.99%	39.61%
ChAPR2	2goy.1.A	52.46%	0.54	0.42	0.77	40.35%	5.54%	14.86%	39.25%
ChAPR3-1	2goy.1.A	54.36%	0.53	0.41	0.76	46.29%	6.55%	13.10%	34.06%
ChAPR3-2	2goy.1.A	54.58%	0.52	0.41	0.75	40.39%	4.15%	14.63%	40.83%

adenine ring, further strengthening the binding between the substrate and the enzyme (Fig. 9A). These structural features are highly similar to the active site structure of AtAPK, indicating commonality in function and catalytic mechanisms [30, 33, 64]. Based on structural comparison, the displacement of the P-loop (Ser^{110}-Thr^{116}) residues and the binding of Mg^{2+} ions play a crucial role in the active site structure of AtAPK, promoting substrate binding and the conformational change of the DGDN-loop, thereby activating the enzyme's catalytic activity [30]. A similar mechanism may also occur in ChAPK, suggesting the important role of Mg^{2+} and specific amino acid residues in regulating the activity of these enzymes. However, molecular docking analysis of ChAPR revealed differences in the interactions of key amino acid residues, which may affect the enzyme's catalytic activity and substrate specificity. For ChAPR1-1, within its CS region, Asp^{131}, Phe^{126}, and Leu^{150} form a hydrogen bond network with the selenate group, enhancing the stability of the interaction between the selenate group and the enzyme. The salt bridge formed between Lys^{209} and the phosphate group may facilitate the precise positioning of the substrate. Ser^{127} and Gly^{226} form hydrogen bonds with the 2'-OH group of the ribose ring, while Gln^{231} interacts with the 3'-OH group, further stabilizing the ribose. Additionally, the π-π interaction between the adenine ring and Arg^{313} may help stabilize the substrate binding, while Ser^{293} forms hydrogen bonds with the NH_2 group of adenine, further strengthening the enzyme-substrate complex. In the MBS region, there is a positional deviation in substrate binding by amino acids. Specifically, Ser^{127} forms a hydrogen bond with the ribose ring, while Arg^{310} and Arg^{313} interact with the 2'-OH and 3'-OH of the ribose ring through hydrogen bonding. Additionally, Gln^{231} and Thr^{225} form hydrogen bonds with the phosphate group, and Asp^{131} forms hydrogen bonds with the selenate group, collectively enhancing the binding stability of selenate and phosphate groups to the enzyme (Fig. 9B).

Effect of selenium on antioxidant enzyme activities of *C. hupingshanensis*

Antioxidant enzymes, including SOD, POD, and CAT, play a key role in protecting plant cells from oxidative damage caused by reactive oxygen species (ROS) [65]. In this study, we investigated the effects of different selenium concentrations on the activity of these enzymes (Fig. 10).

SOD activity exhibited distinct dynamic responses under different selenium concentrations (Fig. 10A). Under low-concentration selenium stress(1 μg Se L^{-1}) and moderate-concentration selenium stress(10 μg Se L^{-1}), SOD activity initially increased, then decreased, and increased again, indicating a fluctuating response to selenium stress (Fig. 10A). Specifically, under low-concentration stress, SOD activity increased by 30.7% on day 1, followed by a decrease on day 3, and then increased again on day 5. Similarly, under moderate-concentration stress, SOD activity showed an increase of 15.8% on day 5 after an initial rise and subsequent decline. In contrast, under high-concentration stress (100 μg Se L^{-1}), SOD activity gradually increased, suggesting that under high selenium stress, plants may initially suppress SOD activity but later activate other antioxidant defense mechanisms to increase SOD activity. On day 1, the low-concentration stress showed significantly higher SOD activity than the other groups, indicating that low selenium stress may initially stimulate SOD activity to mitigate cellular damage.

CAT activity increased with higher selenium concentrations (1 μg Se L^{-1}, 10 μg Se L^{-1}, 100 μg Se L^{-1}), reflecting an enhanced antioxidant defense response in the plant (Fig. 10C). Under low-concentration selenium stress (1 μg Se L^{-1}), CAT activity remained lower than in the control group at all time points, suggesting that under low-concentration stress, the plants may rely on other antioxidant mechanisms rather than CAT activity. Moderate-concentration selenium stress (10 μg Se L^{-1}), CAT activity increased by approximately 20% on day 3. However, it decreased by around 30% on day 5, indicating

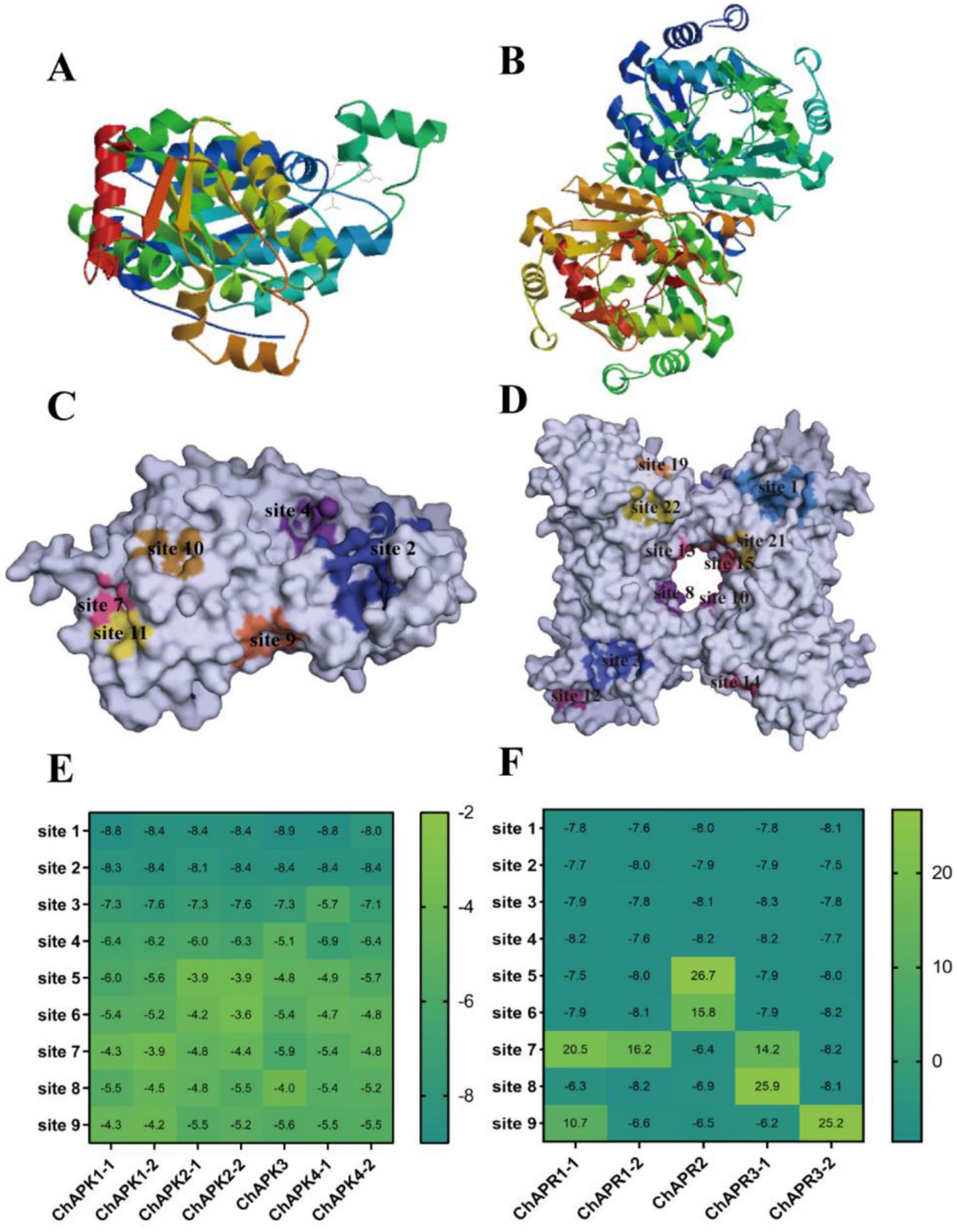

Fig. 7 Predicted three-dimensional structures of the proteins by the SWISS-MODEL server, visualization of predicted ligand-binding sites by PrankWeb for the proteins, and binding energies of ChAPK with APSe and ChAPR with APSe, with genes represented at the bottom of the heat map, the vertical axis showing ligand-binding sites, and values representing the binding energies from ligand-protein docking, units: kcal·mol^{-1} (**A, C, E**) ChAPK. (**B, D, F**) ChAPR

a transient activation of CAT followed by a shift to other defense mechanisms as the stress persisted. Under high-concentration selenium stress (100 μg Se L^{-1}), CAT activity peaked on day 1, with a 30% increase compared to the control, before declining by approximately 40% by day 5. This pattern suggests an initial activation of CAT to cope with acute stress, followed by a reduction as other antioxidant systems became more involved. Overall, these changes in CAT activity reflect a concentration-dependent response to selenium stress, characterized by

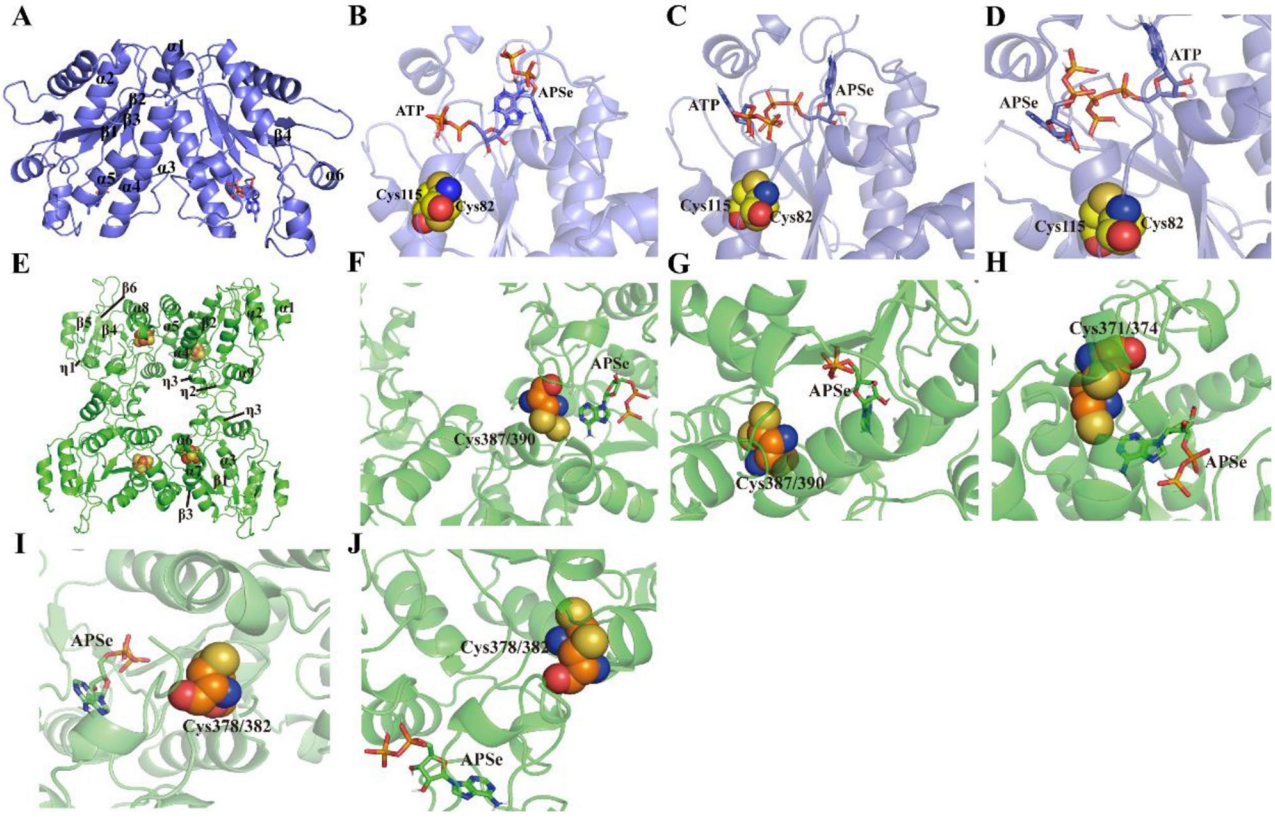

Fig. 8 Structural overview of ChAPK and ChAPR. (**A**) The dimer of the ChAPK is displayed as a cartoon slate diagram, with α-helices and β-strands labeled. (**B**) Diagram showing the potential disulfide bond binding sites of ChAPK1-1. (**C**) Diagram showing the potential disulfide bond binding sites of ChAPK1-2. (**D**) Diagram showing the potential disulfide bond binding sites of ChAPK4-2. (**E**) The dimer of the ChAPR is displayed as a cartoon slate diagram, with α-helices and β-strands labeled. (**F**) Diagram showing the potential disulfide bond binding sites of ChAPR1-1. (**G**) Diagram showing the potential disulfide bond binding sites of ChAPR1-2. (**H**) Diagram showing the potential disulfide bond binding sites of ChAPR2. (**I**) Diagram showing the potential disulfide bond binding sites of ChAPR3-1. (**F**) Diagram showing the potential disulfide bond binding sites of ChAPR3-2.

distinct patterns of activation and downregulation as the plants adapt to the stress.

Similar to CAT activity, POD activity increased with higher selenium treatment concentrations (1 μg Se L^{-1}, 10 μg Se L^{-1}, 100 μg Se L^{-1}), suggesting that POD plays a key role in ROS elimination, thereby mitigating oxidative stress (Fig. 10B). Under high-concentration stress, POD activity was significantly higher than in other treatment groups on day 1, maintaining a consistently elevated level throughout the treatment period. This suggests a full activation of POD to combat oxidative damage under high-concentration stress. In contrast, although POD activity in the low-concentration and moderate-concentration stress groups showed an upward trend, it remained lower than in the control group. Specifically, the low-concentration stress group, POD activity increased by approximately 16% on day 3 but remained about 6% lower than the control on day 5. The moderate-concentration stress group, POD activity rose by about 47% on day 3, then decreased by 21% by day 5, indicating a transient response to selenium stress. Overall, the changes in POD activity suggest that plants activate more complex antioxidant system to cope with selenium stress.

ROS-scavenging-related compounds in *C. hupingshanensis*

H_2O_2, a reactive oxygen species (ROS), is commonly used to assess oxidative stress in plants, with changes in its concentration reflecting cellular oxidative pressure [66]. MDA, a product of lipid peroxidation, serves as an indicator of cell membrane damage and oxidative injury. GSH, and its oxidized form, GSSG, are key markers of the plant's redox status [67]. The GSH/GSSG ratio, with a higher value indicating better antioxidant capacity, is widely used to assess the intracellular reduction state. These metabolites offer valuable insights into the effects of different selenium concentrations on the plant's antioxidant system (Fig. 11). The H_2O_2 content in *C. hupingshanensis* leaves increased with rising selenium treatment concentrations (Fig. 11A). Under low-concentration selenium stress (1 μg Se L^{-1}), H_2O_2 content increased by 33.61%, suggesting that low-concentration stress did not effectively activate the antioxidant defense, leading to H_2O_2 accumulation. In contrast,

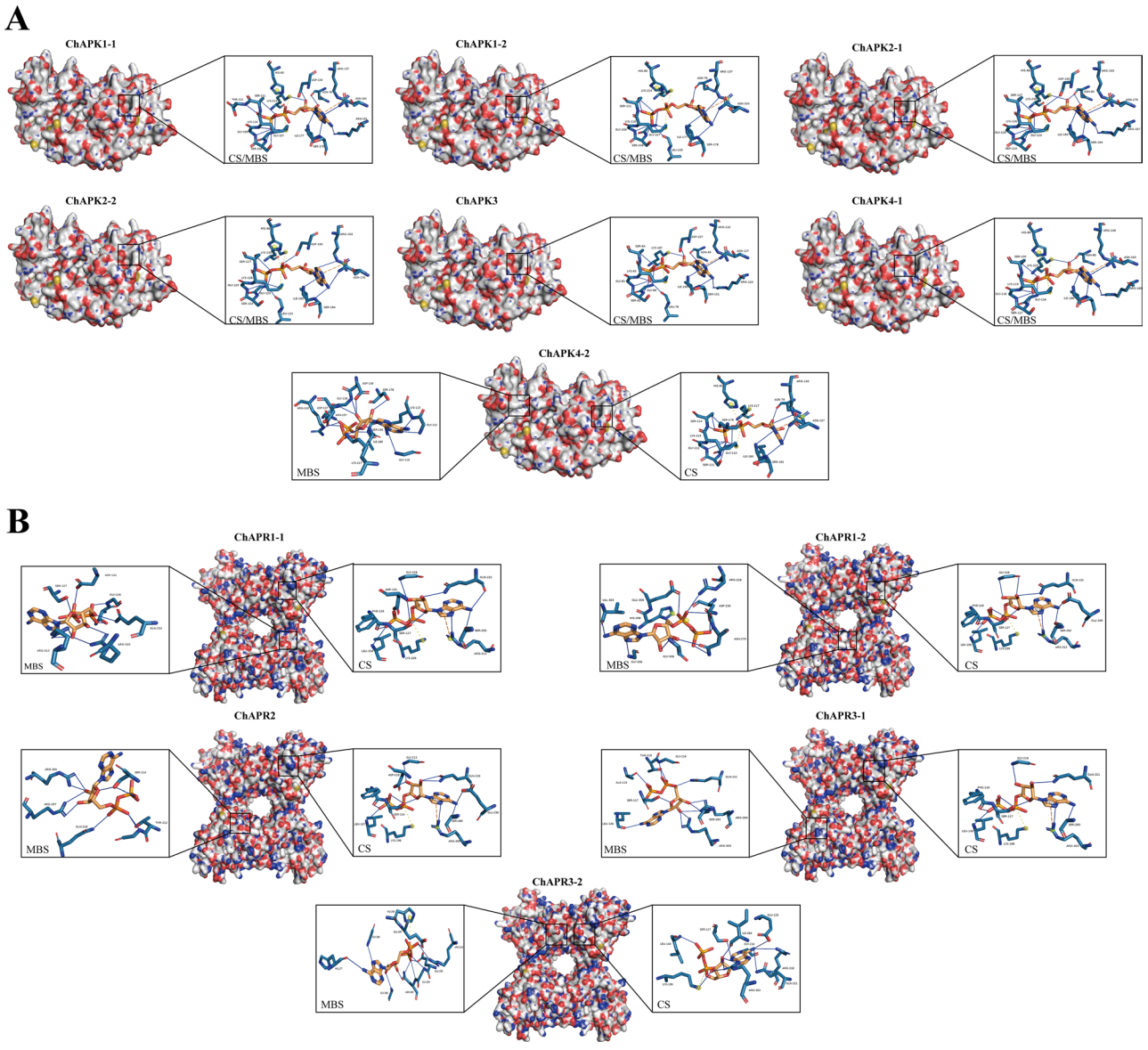

Fig. 9 Interactions of the APK and APR enzymes and ligands. The left panel is the overall view, and the right panel is the focused view. The enzyme is shown on the surface, with binding site amino acid residues and ligands in black. The green dashed lines represent hydrophobic interactions and the black dashed lines represent hydrogen bonds. (**A**) ChAPK: Interactions of the binary ChAPK-ATP complex with APSe. (**B**) ChAPR: Interactions of the binary ChAPR-ATP complex with APSe. CS: putative binding mode of APK and APR enzymes and ligands to model the protein structure at the catalytic site. MBS: APK and APR enzymes and ligands are in a putative binding mode that mimics the protein structure at the site of minimum binding energy, the site of maximum affinity binding

the moderate-concentration selenium stress (10 μg Se L^{-1}) showed a 77.87% increase, likely activating the antioxidant enzyme system to convert ROS into H_2O_2. However, high-concentration selenium (100 μg Se L^{-1}), H_2O_2 content increased by 89.19% by day 5, indicating that prolonged oxidative stress might overwhelm the antioxidant defense system, potentially exacerbated by selenium toxicity. These results suggest that while optimal selenium concentrations can enhance the plant's antioxidant capacity, excessively high selenium levels may be harmful. We also examined changes in MDA content at different concentrations and time points (Fig. 11B). Specially, the MDA content in the leaves with both low-concentration selenium stress (1 μg Se L^{-1}) and high-concentration selenium stress (100 μg Se L^{-1}) gradually increased over time. under low-concentration stress, the antioxidant defense system was insufficient to manage oxidative stress, leading to lipid peroxidation and MDA accumulation. On day 5, MDA content under low-concentration stress increased by 26.89% compared to the control group, reflecting inadequate antioxidant defense. Under high-concentration selenium stress (100 μg Se

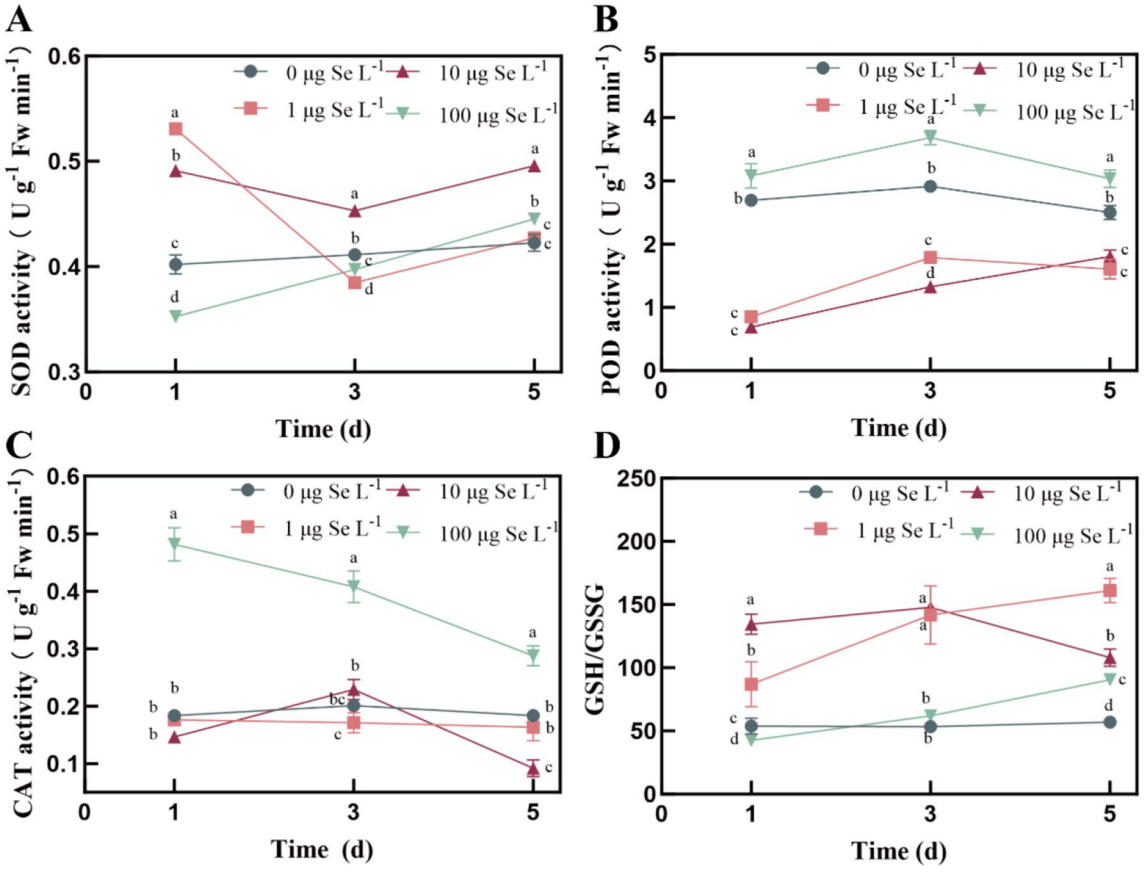

Fig. 10 Changes in antioxidant enzyme activity in the leaves of *C. hupingshanensis* seedlings treated with different concentrations of selenium (0 μg Se L^{-1}, 1 μg Se L^{-1}, 10 μg Se L^{-1}, 100 μg Se L^{-1}) (**A**) CAT (**B**) POD (**C**) SOD (**D**) GSH/GSSG. Each dot represents the mean ± SD (standard derivation) of three replicates. (a, b, c) indicate significant differences observed on different days after selenium treatment ($P < 0.05$)

L^{-1}), MDA content increased significantly over time, with a 47.12% rise on day 1 and a further increase of 41.52% on day 3. These sustained increases suggest that oxidative stress continues to surpass the plant's antioxidant defense capacity, leading to sustained lipid peroxidation and cellular damage. This indicates that excessive selenium concentrations may impair the plant's ability to mitigate oxidative damage. The GSH/GSSG ratios is a key indicator of cellular redox status, with a higher ratio indicating a reduced state and a lower ratio indicating an oxidized state (Fig. 10D). In the control group, the GSH/GSSG ratio remained stable, reflecting a balanced redox environment. Under low-concentration selenium stress (1 μg Se L^{-1}), the GSH/GSSG ratio increased by 90.9% on day 1, suggesting a more reduced cellular environment maintained over time, likely due to increased GSH synthesis to counteract oxidative stress. In contrast, the moderate-concentration selenium stress (10 μg Se L^{-1}) showed an initial increase in the ratio by 12.8% on day 1, followed by a significant decrease of 20.5% on day 3. This pattern suggests that the plant's antioxidant defenses were initially activated, but the reducing agents were eventually depleted, leading to a more oxidized environment (Fig. 11C and D). In the high-concentration selenium stress (100 μg Se L^{-1}), the GSH/GSSG ratio was initially lower than the control group but gradually increased by 15.6% by day 5. The increase suggeststhat the plant adapted to oxidative stress by synthesizing more GSH, helping to counterbalance the oxidative state within the cells.

Based on a comprehensive analysis of the data presented, it was observed that under low-concentration stress, the GSH/GSSG ratio remained high, and the activity of antioxidant enzymes was stable or showed a slight increase, while the contents of H_2O_2 and MDA did not rise significantly. This suggests that the cells were in a reduced state with effectively managed oxidative stress. Under moderate-concentration stress, minor changes were noted in the activity of antioxidant enzymes and the content of H_2O_2 and MDA, indicating that the cells may have maintained a balance between oxidative and reductive states. Under high-concentration stress, although the GSH/GSSG ratio initially decreased and later recovered, the observed increase in H_2O_2 and MDA contents, along with a reduction in CAT activity, suggests that the cells were likely experiencing oxidative stress.

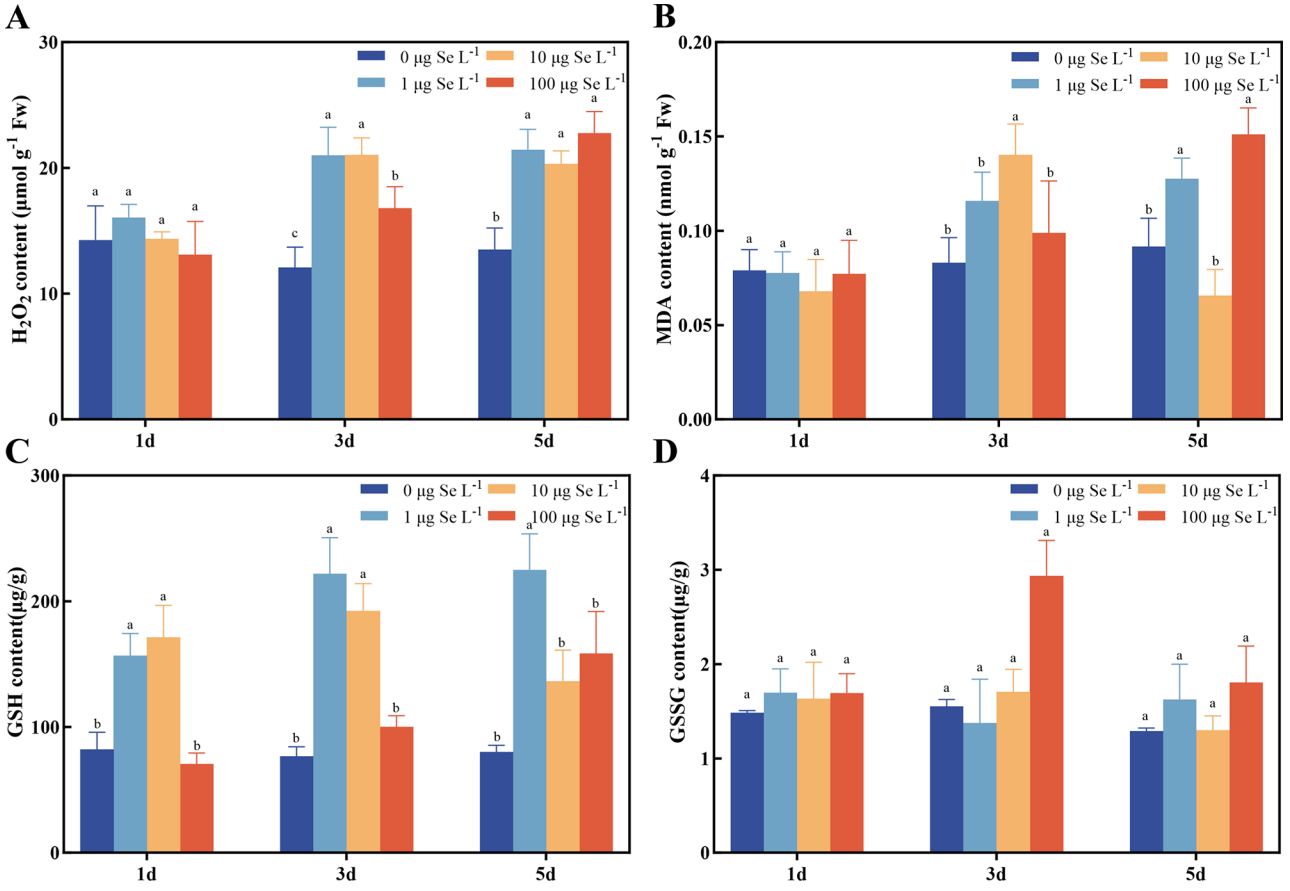

Fig. 11 Changes in GSH and GSSG content in the leaves of *C. hupingshanensis* seedlings treated with selenium in different concentrations (0 μg Se L^{-1}, 1 μg Se L^{-1}, 10 μg Se L^{-1}, 100 μg Se L^{-1}) (**A**) H_2O_2 (**B**) MDA (**C**) GSH (**D**) GSSG. Each dot represents the mean ± SD (standard derivation) of three replicates. (a, b, c) indicate significant differences observed on different days after selenium treatment ($P < 0.05$).

Expressions analysis of *ChAPK* and *ChAPR* genes in leaf tissues under Se stress

To further investigate the molecular functions of *ChAPK* and *ChAPR* genes under short-term selenium stress, the RT q-PCR technique was employed to analyze gene expression changes in leaf tissues exposed to low-concentration selenium stress (1 μg Se L^{-1}) and high-concentration selenium stress (100 μg Se L^{-1}). This analysis aimed to assess the expression profiles of the *ChAPK* and *ChAPR* genes in response to selenium stress. Time points were selected to capture the dynamic responses of the genes at different stages of stress. The results indicate that *ChAPK* gene family members exhibited a significant upregulation in expression at 3 h of low-concentration stress, with expression levels higher than those under high-concentration stress. For example, the expression of *ChAPK2-1* increased approximately 4.2-fold under low-concentration stress, whereas it only increased about 1.6-fold under high-concentration stress.This suggests that low-concentration stress may prompt the genes to respond rapidly and upregulate their expression under a reduced state, whereas high- concentration stress might suppress expression. Notably, *ChAPK4-2* showed an opposite expression trend at 3 h, suggesting that this gene may not play a major role under this stress condition. At the 6 h, with the exception of *ChAPK4-2*, most *ChAPK* gene family members exhibited higher expression levels under high-concentration stress compared to low-concentration stress. For example, the expression of *ChAPK1-1* was 1.72 times higher under high-concentration stress than under low-concentration stress. This phenomenon may suggest that high-concentration selenium stress, by inducing changes in oxidative state, further enhances the expression of certain genes. At 24 h, with the exception of *ChAPK2-1*, *ChAPK2-2*, and *ChAPK4-1*, the expression of other genes was higher under high-concentration stress than under low-concentration stress, which could be due to the oxidative state at high concentrations promoting a greater role of these genes.

For the *ChAPR* gene family members, under low-concentration stress, the gene expression increased continuously with time and peaked at 24 h, higher than under high-concentration stress. For example, the expression of *ChAPR2* increased approximately 10.1-fold under

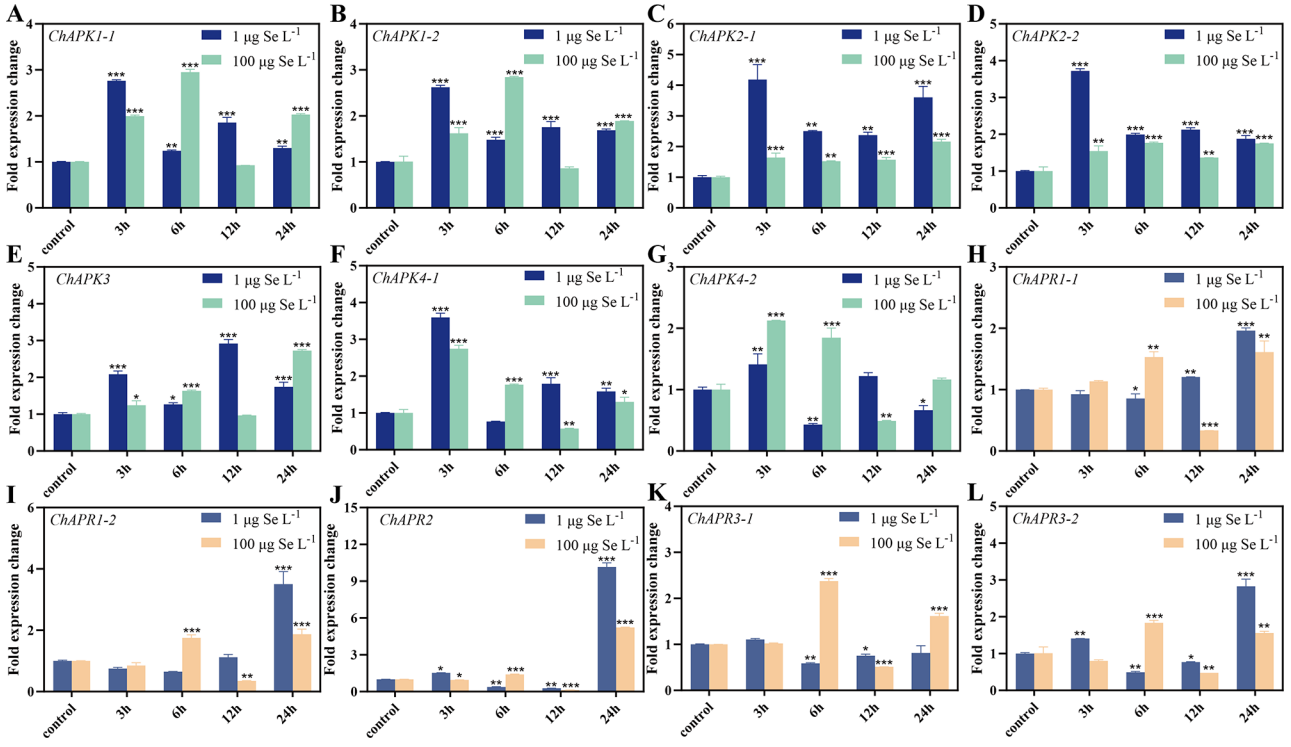

Fig. 12 Fold expression changes of *ChAPK* and *ChAPR* genes in leaves under different selenium treatments (1 μg Se L^{-1} and 100 μg Se L^{-1}). Gene expression was normalized using *Chactin* as the reference gene, and Fold expression changes of the control samples were set to 1. Dark blue and green represent *ChAPK*, while light blue and flesh represent *ChAPR*. (**A**) Fold expression changes of *ChAPK1-1*. (**B**) Fold expression changes of *ChAPK1-2*. (**C**) Fold expression changes of *ChAPK2-1*. (**D**) Fold expression changes of *ChAPK2-2*. (**E**) Fold expression changes of *ChAPK3*. (**F**) Fold expression changes of *ChAPK4-1*. (**G**) Fold expression changes of *ChAPK4-2*. (**H**) Fold expression changes of *ChAPR1-1*. (**I**) Fole expression changes of *ChAPR1-2*. (**J**) Fold expression changes of *ChAPR2*. (**K**) Fold expression changes of *ChAPR3-1*. (**L**) Fold expression changes of *ChAPR3-2*. Each data point represents the mean ± standard deviation (SD) ($n = 3$). * ($P \le 0.05$), ** ($P \le 0.01$), *** ($P \le 0.001$) indicated significant difference in Duncan's test

low-concentration stress and 5.2-fold under high-concentration stress. However, *ChAPR3-1* exhibited significantly higher expression at 24 h under high-concentration stress, suggesting that this gene may be one of the key genes responding to high-concentration oxidative stress, or it may have different response characteristics. Additionally, at 6 h, the expression of *ChAPR* gene family members under low-concentration stress was lower than under hig-concentration stress. This may be because high-concentration stress induce stronger oxidative stress, thereby activating *ChAPR* family genes to enhance the plant's antioxidant capacity, resulting in higher gene expression at high-concentration conditions (Fig. 12).

Discussion

APK and APR, as key enzymes in the primary and secondary branches of sulfur metabolism, play an important role in sulfur allocation regulation [30]. As explained by RenWei et al., due to the similar chemical properties of selenium and sulfur, plants generally absorb and metabolize selenium through the sulfur metabolic pathway [68]. Therefore, APK and APR also play a significant role in plant selenium metabolism. The *APK* and *APR* gene families have been comprehensively identified in various animals, plants, and bacteria (*A. thaliana*, *V. vitifera*, *O. sativa*, *Z. mays*, *Catharanthus roseus*, *Allium cepa L*, *Chlamydomonas reinhardtii*, *Enteromorpha intestinalis*) [34, 69–71]. However, a comprehensive study of *APK* and *APR* genes in *C. hupingshanensis* has not yet been conducted. Our study aims to fill this gap by identifying the *APK* and *APR* genes in the genome of this species and performing thorough characterization, including phylogenetic relationships, their physicochemical properties, molecular docking simulations of substrate affinity, and expression levels under different selenium concentrations.

Similar to AtAPK and AtAPR, multiple sequence alignment analysis revealed that ChAPK and ChAPR possess target disulfide bonds regulated by the redox state of cells or organelles. This finding is consistent with similar structural features observed in *A. thaliana* (*AtAPK*) and rise (*OsAPK*) [30, 34]. In ChAPK1-1 (ChAPK1-2), C82 and C115 are predicted as potential disulfide bond formation sites, whereas in ChAPK4-2, C91 and C124 are identified as potential sites for disulfide bond formation (Fig. 8B, C and D). This is similar to findings in *OsAPK*,

where disulfide bond formation in the presence of GSSG leads to a reduction in enzyme activity [34]. However, not all ChAPK proteins are regulated by redox mechanisms, and some APK proteins may be influenced by other regulatory factors. Specifically, mutations at potential disulfide bond-forming sites (such as the cysteine-to-phenylalanine mutation in ChAPK2-1 and ChAPK2-2, and the serine mutation in ChAPK3) could interfere with the redox regulation of these proteins, thus affecting enzyme activity. This phenomenon is similar to previous findings in AtAPK1 mutants (C86A/C119A), where kinetic properties and enzyme activity under reducing conditions were found to resemble those of the wild-type (WT) enzyme [30]. Therefore, although redox regulation is an important mechanism for ChAPK proteins, not all proteins rely on this mechanism, and there are differences due to other regulatory factors or distribution patterns. For example, *ChAPK3*, localized in the cytoplasm, typically exhibits low expression levels, which may be attributed to its unique regulatory mechanisms and functional specialization. Selenium metabolism occurs in both the cytoplasm and plastids of plants, and the low expression of *ChAPK3* could reflect a functional partitioning and redundancy with other *ChAPKs*. However, the role of *ChAPK3* remains indispensable, specifically in providing PAPSe for selenylation reactions within the cytoplasm. Additionally, its expression may be tissue or developmentally specific. For example, *AtAPK3* is highly expressed in pollen, but shows reduced expression in other tissues [81]. Therefore, the overall lower expression of *ChAPK3* could be due to its specialized function in certain tissues, such as reproductive organs, rather than in leaves. The *ChAPR* gene family members exhibit a high degree of conservation, particularly in the redox-active motif at the C-terminus (CxxC), suggesting that these members share similar functions and mechanisms of action (Fig. 8F and J). Previous studies have shown that the catalytic efficiency of APR is regulated by its oxidation state, where GSH reduces the C-terminal domain and forms a disulfide bond [31], leading to enzyme inactivation. Therefore, *ChAPR* may also be influenced by its redox state, which could promote the formation of disulfide bonds and regulate its enzymatic activity [29, 40, 72]. Based on these similar findings, it is hypothesized that *ChAPK* and *ChAPR* are also regulated by their redox state, which in turn affects their enzymatic activity.

The primary and secondary metabolic pathways of selenium metabolism in *C. hupingshanensis* are regulated by the *APK* and *APR* gene families, respectively, involving both primary and secondary metabolic processes. Previous studies have found that in *A. thaliana*, three *APR* genes are involved in primary metabolism, primarily responsible for sulfur reduction and cysteine synthesis, while four *APK* genes regulate the synthesis and accumulation of sulfur donors in secondary metabolism [69, 73]. Given the similar chemical properties of sulfur (S) and selenium (Se) [68], the expression of *ChAPK* and *ChAPR* family genes may regulate the flow of selenium metabolism and coordinate the balance between these two metabolic pathways. Previous studies have confirmed that APR generates cysteine, a key precursor for the synthesis of GSH, which acts as an important antioxidant in cells, helping maintain redox balance and prevent oxidative damage [25] (Fig. 1). Biochemical studies have also confirmed that the enzyme activity decreases in the reduced state [31]. In this study, the expression of *ChAPR* gene family members gradually increased under low concentration (1 μg Se L^{-1}) stress, peaking at 24 h. Since it can participate in the reduction of selenate to cysteine, enhancing GSH synthesis, it helps the plant cope with low selenium concentration stress. Therefore, the upregulation of its expression could be a strategy to enhance antioxidant capacity and improve stress responses. However, the expression of *ChAPR3-1* did not change significantly, which may suggest that this gene is not directly involved in the selenium stress response, or its regulatory mechanism differs from that of other members. Physiological indicators revealed a significant increase in SOD enzyme activity at 24 h. However, considering other indicators, such as the increased intracellular GSH/GSSG ratio, relatively stable CAT and POD enzyme activities, and no significant increase in H_2O_2 and MDA levels, it suggests that the plant's antioxidant mechanisms are effectively controlled, further supporting this hypothesis. In contrast to *ChAPR*, *ChAPK* gene family members were rapidly upregulated at the early stage of stress (3 h) and then gradually returned to levels close to the initial state. This suggests that *ChAPK* plays a key role in the early stages of stress, responding to oxidative stress by synthesizing selenate donors. Studies have also confirmed that *AtAPK* activity increases under excessive GSH conditions, suggesting that the enzyme activity is high at this point [31]. Therefore, *ChAPK* may not need to maintain high expression levels over a long period, or it may return to normal levels through other regulatory mechanisms. However, under high concentration (100 μg Se L^{-1}) stress, the expression of *ChAPR* gene family members first increased and then decreased at the early stage of stress (6 h), with a significant increase at 24 h compared to the normal level. Similarly, the expression of *ChAPK* gene family members showed a similar trend.This may suggest that under high selenium concentration stress, *ChAPR* rapidly activates the selenium reduction and cysteine synthesis pathways to mitigate selenium toxicity, while *ChAPK* quickly initiates the synthesis pathway of selenate donors to cope with selenium accumulation and stress. Previous studies have confirmed that *AtAPR* enzyme activity is activated by

oxidation, suggesting that *ChAPR* may also have similar oxidative activation properties [31]. Physiological indicator analysis showed increased CAT and POD enzyme activity at 24 h, decreased SOD enzyme activity, no significant increase in H_2O_2 and MDA levels, but a slightly lower GSH/GSSG ratio compared to the control group. This result suggests that the higher GSSG content in the plant may promote APR enzyme activity, thereby coping with high selenium stress. The expression of *ChAPK4-2* at 24 h was not significantly higher than that of the control group, suggesting that this gene may not directly participate in the response to high selenium concentration stress or may have functional redundancy.

Conclusion

We conducted a comprehensive analysis of the *ChAPK* and *ChAPR* gene families, identifying a total of 7 *ChAPK* and 5 *ChAPR*. Multiple sequence alignment analysis revealed that *ChAPK1-1*, *ChAPK1-2*, *ChAPK4-2*, and all *ChAPR* gene members contain potential disulfide bond-forming sites, which may be regulated by the redox state. The significant increase in antioxidant enzyme activity suggests that selenium can enhance the plant's antioxidant defense mechanisms. Furthermore, analysis of oxidative metabolites indicates that low selenium concentration (1 μg Se L^{-1}) has a promotive effect, while high concentration (100 μg Se L^{-1}) exhibits stress effects. Based on short-term gene expression analysis, we found that under low selenium concentration (1 μg Se L^{-1}), the primarily expressed gene is *ChAPK2-1*, which does not form disulfide bonds, while under high selenium stress, *ChAPK1-1*, which forms disulfide bonds, is mainly expressed. Additionally, *ChAPR2* exhibited significant expression under both selenium concentrations, suggesting its potential key role in the selenium stress response. In conclusion, selenium may play a critical role in antioxidant responses and selenium metabolism in plants by regulating the expression of *ChAPK* and *ChAPR* gene families. This role may involve redox regulation and the activation of antioxidant enzymes.

Supplementary Information

The online version contains supplementary material available at https://doi.org/10.1186/s12870-025-06555-1.

Supplementary Material 1: Table S1: The coding sequences and protein sequences of ChAPK and ChAPR genes

Supplementary Material 2: Table S2: The primers of ChAPK and ChAPR genes for qRT-PCR

Supplementary Material 3

Supplementary Material 4: Fig. S1: Multiplexed alignment of full sequences of APK and APR protein in C. hupingshanensis

Acknowledgements
We express our heartfelt gratitude to all colleagues who have dedicated their unwavering efforts to the successful execution of these experiments.

Author contributions
Conceptualization: Yue Xu, Lilong Gao, Yifeng Zhou and Qiaoyu Tang; Methodology: Yue Xu, Lilong Gao, Yifeng Zhou and Qiaoyu Tang; Software: Yue Xu, Jingyi Liu, Wenwu Guan, Jingyu Xie; Validation: Yifeng Zhou, Yanke Lu and Zhi Hou; Formal analysis: Yanke Lu, Zhi Hou and Zhixin Xiang; Investigation: Yue Xu and Yifeng Zhou; Resources: Jingyi Liu and Wenwu Guan; Data curation: Yue Xu; Writing—original draft preparation: Yue Xu; Visualization: Yue Xu, Lilong Gao, Xixi Zeng and Yushan Chen; Supervision: Yifeng Zhou; Funding acquisition: Yifeng Zhou and Qiaoyu Tang. All authors have read and agreed to the published version of the manuscript.

Funding
This work was supported by the National Natural Science Foundation of China (32260070), the Excellent Young and Middle-aged Scientific and Technological Innovation Team Projects of Colleges and Universities in Hubei Province (T2020020) and the Open Fund of Hubei Key Laboratory of Biological Resources Protection and Utilization (KYPT012301) to Yifeng Zhou and Qiaoyu Tang. The research was mainly finished at the Hubei Key Laboratory of Biological Resources Protection and Utilization. This research was also supported by the the innovation project for graduate education of Hubei Minzu University (MYK2024005).

Data availability Statement
The data that support the findings of this study are available from the corresponding author upon reasonable request.

Declarations

Ethics approval
Not applicable.

Consent for publication
Not applicable.

Conflict of interests
The authors declare no competing interests.

Author details
[1]Hubei Key Laboratory of Biological Resources Protection and Utilization, Hubei Minzu University, Enshi 44500, China
[2]Collage of Biological and Food Engineering, Hubei Minzu University, Enshi 44500, China
[3]Collage of Forestry and Horticulture, Hubei Minzu University, Enshi 44500, China

Received: 7 November 2024 / Accepted: 14 April 2025
Published online: 22 May 2025

References

1. Kieliszek M, Bano I, Zare H. A comprehensive review on selenium and its effects on human health and distribution in middle Eastern countries. Biol Trace Elem Res. 2022;200(3):971–87.
2. Chauhan R, Awasthi S, Srivastava S, Dwivedi S, Pilon-Smits EA, Dhankher OP, Tripathi RD. Understanding selenium metabolism in plants and its role as a beneficial element. Crit Rev Environ Sci Technol. 2019;49(21):1937–58.
3. Huang S, Qin H, Jiang D, Lu J, Zhu Z, Huang X. Bio-nano selenium fertilizer improves the yield, quality, and organic selenium content in rice. J Food Compos Anal 2024:106348.
4. Zhu J, Yue Z, Ahsan MZ, Lao D, Panhwar FH, Ling L, Yang S, Jia X, Ye X, Rongjun C. Dynamics of Selenium-Mercury Interaction Under Hg Stress in High and Low Selenium Rice Genotypes. *Available at SSRN 4804982*.
5. Lu B, An H, Song X, Yang B, Jian Z, Cui F, Xue J, Gao Z, Du T. Enhancement of nutritional substance, trace elements, and pigments in waxy maize grains through foliar application of selenite. Foods. 2024;13(9):1337.

6. Mrština T, Praus L, Száková J, Kaplan L, Tlustoš P. Foliar selenium biofortification of soybean: the potential for transformation of mineral selenium into organic forms. Front Plant Sci. 2024;15:1379877.
7. Golubkina N, Kharchenko V, Moldovan A, Antoshkina M, Ushakova O, Sękara A, Stoleru V, Murariu OC, Tallarita AV, Sannino M. Effect of selenium and Garlic extract treatments of seed-Addressed lettuce plants on biofortification level, seed productivity and mature plant yield and quality. Plants. 2024;13(9):1190.
8. Collado-González J, Piñero MC, Otálora Alcón G, López-Marín J, Del Amor FM. Biofortification and valorization of celery byproducts using selenium and PGPB under reduced nitrogen regimes. Foods. 2024;13(10):1437.
9. Alotaibi MO, Alotibi MM, Majrashi DM, Mahmoud E, Ghoneim AM, Eissa MA, Tammam SA. Effect of selenium form and dose on Camelthorn (*Alhagi maurorum Medik*) grown on a metal-contaminated soil. Environ Sci Pollut Res 2024:1–10.
10. Liu J, Liu J, Aamer M, Liao Y, Yang Y, Yao F, Zhu B, Gao Z, Cheng C. Regulating effect of sodium selenite addition on seed germination and growth of pepper (*Capsicum annuum L.*) under mixed salt stress. J Soil Sci Plant Nutr 2024:1–11.
11. Hajlaoui F, Hajlaoui H, Krouma A. Physio-Biochemical Response to Exogenous Selenium Application of Tomatoes (*Solanum lycopersicum L.*) Cultivated in the Field under Saline Irrigation. Russ J Plant Physiol. 2023;70(6):142.
12. Zhong Y, Cui H, Li H, Qiang X, Han Q, Liu H. Foliar application of selenium enhances drought tolerance in tomatoes by modulating the antioxidative system and restoring photosynthesis. Agronomy. 2024;14(6):1184.
13. Wen D, Zheng Y, Han Y, Song J, Sun S, Yang N, Wang X. Sodium selenite increases drought tolerance by promoting jasmonic acid biosynthesis in cucumber. Hortic Adv. 2023;1(1):6.
14. Shahid M, Saleem MF, Saleem A, Sarwar M, Raza MAS, Anjum SA, Hussain A. Sustainable production of bread wheat under terminal heat stress: an investigation of foliar selenium-mediated biochemical regulations in association with yield. Cereal Res Commun. 2024;52(2):671–81.
15. Sita K, Sehgal A, Kumar S, Nayyar H. Individual and combined effects of selenium and silica on enhancing the heat tolerance of lentil (*Lens culinaris Medik.*) genotypes. Plant Physiol Rep. 2022;27(3):481–97.
16. Jiang X, Zhou W, Li D, Wang H, Yang Y, You J, Liu H, Ai L, Zhang M. Combined transcriptome and metabolome analyses reveal the effects of selenium on the growth and quality of *Lilium lancifolium*. Front Plant Sci. 2024;15:1399152.
17. Ikram S, Li Y, Lin C, Yi D, Heng W, Li Q, Tao L, Hongjun Y. Weijie JJJoPP: selenium in plants: A nexus of growth, antioxidants, and phytohormones. J Plant Physiol 2024:154237.
18. Schiavon M, Pilon-Smits EA. The fascinating facets of plant selenium accumulation–biochemistry, physiology, evolution and ecology. New Phytol. 2017;213(4):1582–96.
19. White PJ. Selenium accumulation by plants. Ann Botany. 2016;117(2):217–35.
20. Bai H-F, Chen L-B, Liu K-M, Liu L-H. A new species of *Cardamine* (Brassicaceae) from Hunan, China. *Novon: A journal for botanical nomenclature* 2008, 18(2):135–7.
21. Xiang J, Ming J, Yin H, Zhu Y, Li Y, Long L, Ye Z, Wang H, Wang X, Zhang F. Anatomy and histochemistry of the roots and shoots in the aquatic selenium hyperaccumulator *Cardamine hupingshanensis* (Brassicaceae). Open Life Sci. 2019;14(1):318–26.
22. Shao S, Deng G, Mi X, Long S, Zhang J, Tang J. Accumulation and Sp.ciation of selenium in *Cardamine* Sp. in Yutangba se mining field, Enshi, China. Chin J Geochem. 2014;33:357–64.
23. Zeng X, Yang S, Li F, Yao Y, Wu Z, Xue Y, Liu Y. Genome-Wide identification of *OsZIPs* in rice and gene expression analysis under manganese and selenium stress. Genes. 2024;15(6):696.
24. Huang C, Ying H, Yang X, Gao Y, Li T, Wu B, Ren M, Zhang Z, Ding J, Gao J. The *Cardamine enshiensis* genome reveals whole genome duplication and insight into selenium hyperaccumulation and tolerance. Cell Discovery. 2021;7(1):62.
25. Zhou Y, Tang Q, Wu M, Mou D, Liu H, Wang S, Zhang C, Ding L, Luo J. Comparative transcriptomics provides novel insights into the mechanisms of selenium tolerance in the hyperaccumulator plant *Cardamine hupingshanensis*. Sci Rep. 2018;8(1):2789.
26. Xiao Z, Lu Y, Zou Y, Zhang C, Ding L, Luo K, Tang Q, Zhou Y. Gene identification, expression analysis and molecular Docking of ATP sulfurylase in the selenization pathway of *Cardamine hupingshanensis*. BMC Plant Biol. 2022;22(1):491.
27. Zeng X, Luo G, Fan Z, Xiao Z, Lu Y, Xiao Q, Hou Z, Tang Q, Zhou Y. Whole genome identification, molecular Docking and expression analysis of enzymes involved in the selenomethionine cycle in *Cardamine hupingshanensis*. BMC Plant Biol. 2024;24(1):199.
28. Chen Y, Li Y, Luo G, Luo C, Xiao Z, Lu Y, Xiang Z, Hou Z, Xiao Q, Zhou Y. Gene identification, expression analysis, and molecular Docking of SAT and OASTL in the metabolic pathway of selenium in *Cardamine hupingshanensis*. Plant Cell Rep. 2024;43(6):148.
29. Telman W, Dietz K-J. Thiol redox-regulation for efficient adjustment of sulfur metabolism in acclimation to abiotic stress. J Exp Bot. 2019;70(16):4223–36.
30. Ravilious GE, Nguyen A, Francois JA, Jez JM. Structural basis and evolution of redox regulation in plant adenosine-5′-phosphosulfate kinase. Proceedings of the National Academy of Sciences. 2012;109(1):309–314.
31. De Bont L, Donnay N, Couturier J, Rouhier N. Redox regulation of enzymes involved in sulfate assimilation and in the synthesis of sulfur-containing amino acids and glutathione in plants. Front Plant Sci. 2022;13:958490.
32. Leung SC, Smith D, Chen R, McCallum JA, McKenzie M, McManus MT. Characterization of adenosine 5′-phospho-sulfate kinase (*APSK*) genes from higher plants. Sulfur metabolism in plants: mechanisms and applications to food security and responses to climate change. Springer; 2012. pp. 67–70.
33. Ravilious GE, Westfall CS, Jez JM. Redox-linked gating of nucleotide binding by the N-terminal domain of adenosine 5′-phosphosulfate kinase. J Biol Chem. 2013;288(9):6107–15.
34. De-zhen W, Guo-guo C, Lu-jia L, Zhao-jun J. Yu-chun R, Mei-hao S: in *vitro* functional study of rice adenosine 5′-phosphosulfate kinase. Rice Sci. 2016;23(3):152–9.
35. Bick J-A, Setterdahl AT, Knaff DB, Chen Y, Pitcher LH, Zilinskas BA, Leustek T. Regulation of the plant-type 5 '-adenylyl sulfate reductase by oxidative stress. Biochemistry. 2001;40(30):9040–8.
36. Westerman S, Stulen I, Suter M, Brunold C, De Kok LJ. Atmospheric H_2S as sulphur source for *Brassica oleracea*: consequences for the activity of the enzymes of the assimilatory sulphate reduction pathway. Plant Physiol Biochem. 2001;39(5):425–32.
37. Vauclare P, Kopriva S, Fell D, Suter M, Sticher L, Von Ballmoos P, Krähenbühl U, Den Camp RO, Brunold C. Flux control of sulphate assimilation in *Arabidopsis thaliana*: adenosine 5′-phosphosulphate reductase is more susceptible than ATP sulphurylase to negative control by thiols. 2002, 31(6):729–40.
38. Mendoza-Cózatl D, Loza-Tavera H, Hernández-Navarro A, Moreno-Sánchez R. Sulfur assimilation and glutathione metabolism under cadmium stress in yeast, protists and plants. FEMS Microbiol Rev. 2005;29(4):653–71.
39. Fritz G, Buchert T, Kroneck PM. The function of the [4fe-4s] clusters and fad in bacterial and archaeal adenylylsulfate reductases: evidence for flavin-catalyzed reduction of adenosine 5′-phosphosulfate. J Biol Chem. 2002;277(29):26066–73.
40. Chen F-F, Chien C-Y, Cho C-C, Chang Y-Y, Hsu C-H. C-terminal redox domain of *Arabidopsis* APR1 is a non-canonical thioredoxin domain with glutaredoxin function. Antioxidants. 2019;8(10):461.
41. Feliciano PR, Carroll KS. Drennan CLJAo: crystal structure of the [4Fe–4S] Cluster-Containing Adenosine-5′-phosphosulfate reductase from Mycobacterium tuberculosis. 2021, 6(21):13756–65.
42. Chen C, Chen H, Zhang Y, Thomas HR, Frank MH, He Y, Xia R. TBtools: an integrative toolkit developed for interactive analyses of big biological data. Mol Plant. 2020;13(8):1194–202.
43. Gasteiger E, Gattiker A, Hoogland C, Ivanyi I, Appel RD, Bairoch A. ExPASy: the proteomics server for in-depth protein knowledge and analysis. Nucleic Acids Res. 2003;31(13):3784–8.
44. Robert X, Gouet P. Deciphering key features in protein structures with the new endscript server. Nucleic Acids Res. 2014;42(W1):W320–4.
45. Tamura K, Stecher G, Kumar S. MEGA11: molecular evolutionary genetics analysis version 11. Mol Biol Evol. 2021;38(7):3022–7.
46. Combet C, Blanchet C, Geourjon C, Deleage G. NPS@: network protein sequence analysis. Trends Biochem Sci. 2000;25(3):147–50.
47. Jendele L, Krivak R, Skoda P, Novotny M, Hoksza D. PrankWeb: a web server for ligand binding site prediction and visualization. Nucleic Acids Res. 2019;47(W1):W345–9.
48. Eberhardt J, Santos-Martins D, Tillack AF, Forli S. AutoDock Vina 1.2. 0: new Docking methods, expanded force field, and python bindings. J Chem Inf Model. 2021;61(8):3891–8.
49. Salentin S, Schreiber S, Haupt VJ, Adasme MF, Schroeder M. PLIP: fully automated protein–ligand interaction profiler. Nucleic Acids Res. 2015;43(W1):W443–7.
50. Schöning-Stierand K, Diedrich K, Fährrolfes R, Flachsenberg F, Meyder A, Nittinger E, Steinegger R. Rarey MJNar: proteins plus: interactive analysis of protein–ligand binding interfaces. Nucleic Acids Res. 2020;48(W1):W48–53.
51. Seeliger D, de Groot BL. Ligand Docking and binding site analysis with PyMOL and Autodock/Vina. J Comput Aided Mol Des. 2010;24(5):417–22.

52. Swift ML. GraphPad Prism, data analysis, and scientific graphing. J Chem Inf Comput Sci. 1997;37(2):411–2.
53. Patra HK, Mishra D. Pyrophosphatase, peroxidase and polyphenoloxidase activities during leaf development and senescence. Plant Physiol. 1979;63(2):318–23.
54. Nickel KS, Cunningham B. Improved peroxidase assay method using leuco 2, 3′, 6-trichloroindophenol and application to comparative measurements of peroxidatic catalysis. Anal Biochem. 1969;27(2):292–9.
55. Xu F, ZHANG DW, Zhu F, Tang H, Lv X, Cheng J, XIE HF. LIN HH: A novel role for cyanide in the control of cucumber (*Cucumis sativus L.*) seedlings response to environmental stress. Plant Cell Environ. 2012;35(11):1983–97.
56. Stewart RR, Bewley JD. Lipid peroxidation associated with accelerated aging of soybean axes. Plant Physiol. 1980;65(2):245–8.
57. Motamedi M, Haghighi M, Goli A. Physiological changes of sweet and hot peppers in vegetative and reproductive growth stages treated by Ca and H_2O_2 under unforeseen heat stresses. Sci Hort. 2019;249:306–13.
58. Alexieva V, Sergiev I, Mapelli S, Karanov E. The effect of drought and ultraviolet radiation on growth and stress markers in pea and wheat. Plant Cell Environ. 2001;24(12):1337–44.
59. Livak KJ. TD Schmittgen 2001 Analysis of relative gene expression data using real-time quantitative PCR and the 2− ΔΔCT method. Methods 25 4 402–8.
60. Ravilious GE, Jez JM. Nucleotide binding site communication in *Arabidopsis thaliana* adenosine 5′-phosphosulfate kinase. J Biol Chem. 2012;287(36):30385–94.
61. Arz HE, Gisselmann G, Schiffmann S, Schwenn JD. A cDNA for adenylyl sulphate (APS)-kinase from *Arabidopsis thaliana*. Biochim Et Biophys Acta (BBA)-Gene Struct Expression. 1994;1218(3):447–52.
62. Saraste M, Sibbald PR, Wittinghofer A. The P-loop—a common motif in ATP- and GTP-binding proteins. Trends Biochem Sci. 1990;15(11):430–4.
63. Bick J-A, Åslund F, Chen Y, Leustek T. Glutaredoxin function for the carboxyl-terminal domain of the plant-type 5′-adenylylsulfate reductase. Proceedings of the National Academy of Sciences. 1998;95(14):8404–8409.
64. Zhang M, Ravilious GE, Hicks LM, Jez JM, McCulla RDJJACS. Redox switching of adenosine-5′-phosphosulfate kinase with photoactivatable atomic oxygen precursors. 2012, 134(41):16979–82.
65. Das K, Roychoudhury AJF. Reactive oxygen species (ROS) and response of antioxidants as ROS-scavengers during environmental stress in plants. 2014, 2:53.
66. Mittler R, Zandalinas SI, Fichman Y, Van Breusegem F. Reactive oxygen species signalling in plant stress responses. Nat Rev Mol Cell Biol. 2022;23(10):663–79.
67. Lanza MGDB, Dos Reis ARJPP. Roles of selenium in mineral plant nutrition: ROS scavenging responses against abiotic stresses. Biochemistry. 2021;164:27–43.
68. Liu H, Xiao C, Qiu T, Deng J, Cheng H, Cong X, Cheng S, Rao S, Zhang YJP. Selenium regulates antioxidant, photosynthesis, and cell permeability in plants under various abiotic stresses: a review. 2022, 12(1):44.
69. Mugford SG, Yoshimoto N, Reichelt M, Wirtz M, Hill L, Mugford ST, Nakazato Y, Noji M, Takahashi H, Kramell R. Disruption of adenosine-5′-phosphosulfate kinase in *Arabidopsis* reduces levels of sulfated secondary metabolites. Plant Cell. 2009;21(3):910–27.
70. Urlaub H, Jankowski G. Sulfate reduction in *Catharanthus roseus* (L.) identification and subcellular localization of a particulate adenosine 5′-phosphosulfate-reducing activity in cells from cell suspension cultures. Planta. 1982;155:154–61.
71. Kopriva S, Koprivova A. Plant adenosine 5′-phosphosulphate reductase: the past, the present, and the future. J Exp Bot. 2004;55(404):1775–83.
72. Kopriva S, Buchert T, Fritz G, Suter M, Benda R, Schunemann V, Koprivova A, Schurmann P, Trautwein AX, Kroneck PM. The presence of an iron-sulfur cluster in adenosine 5′-phosphosulfate reductase separates organisms utilizing adenosine 5′-phosphosulfate and phosphoadenosine 5′-phosphosulfate for sulfate assimilation. J Biol Chem. 2002;277(24):21786–91.
73. Setya A, Murillo M, Leustek T. Sulfate reduction in higher plants: molecular evidence for a novel 5′-adenylylsulfate reductase. Proc Natl Acad Sci. 1996;93(23):13383–8.
74. Federhen S. The NCBI taxonomy database. Nucleic Acids Res. 2012;40(D1):D136–43.
75. Yang M, Derbyshire MK, Yamashita RA, Marchler-Bauer A. NCBI's conserved domain database and tools for protein domain analysis. Curr Protoc Bioinformatics 2020;69(1):e90.
76. Horton P, Park K-J, Obayashi T, Fujita N, Harada H, Adams-Collier C, et al. WoLF PSORT: protein localization predictor. Nucleic Acids Res. 2007;35(suppl_2):W585–7.
77. Bailey TL, Boden M, Buske FA, Frith M, Grant CE, Clementi L, et al. MEME SUITE: tools for motif discovery and searching. Nucleic Acids Res. 2009;37(suppl_2):W202–8.
78. Finn RD, Mistry J, Schuster-Böckler B, Griffiths-Jones S, Hollich V, Lassmann T, et al. Pfam: clans, web tools and services. Nucleic Acids Res. 2006;34(suppl_1):D247–51.
79. Thompson JD, Gibson TJ, Higgins DG. Multiple sequence alignment using ClustalW and ClustalX. Curr Protoc Bioinform. 2003(1):2.3. 1–2.3. 22.
80. Zhang H, Gao S, Lercher MJ, Hu S, Chen W-H. EvolView, an online tool for visualizing, annotating and managing phylogenetic trees. Nucleic Acids Res. 2012;40(W1):W569–72.
81. Mugford SG, Matthewman CA, Hill L, Kopriva SJFL. Adenosine-5′-phosphosulfate kinase is essential for arabidopsis viability. 2010;584(1):119–23.

Publisher's note